

Exploiting anisotropic Rashba effects on real-time photocurrents and spin polarization for transient symmetry breaking

Matisse Wei-Yuan Tu*

*Fritz Haber Center for Molecular Dynamics, Institute of Chemistry,
The Hebrew University of Jerusalem, Jerusalem 91904 Israel and
Center for Theoretical and Computation Physics, Department of Physics,
National Sun Yat-sen University, Kaohsiung 80424, Taiwan*

Jyh-Pin Chou

Department of Physics, National Changhua University of Education, Changhua 50007, Taiwan

Chih-Wei Luo

*Department of Electrophysics and Institute of Physics,
National Yang Ming Chiao Tung University, Hsinchu 30010, Taiwan
National Synchrotron Radiation Research Center, Hsinchu 30076, Taiwan and
Taiwan Consortium of Emergent Crystalline Materials (TCECM),
National Science and Technology Council, Taipei 10601, Taiwan*

We theoretically investigate the real-time transient responses of a two-dimensional (2D) electron gas with anisotropic Rashba spin-orbit coupling (SOC) to laser pulses. Through explicitly monitoring the time-dependent photocurrents and spin polarization under different linear polarizations of the laser pulse, we find that the transient breaking of the mirror symmetry in combination with the anisotropy of the Rashba SOC results in significant distinction between the charge-mediated and the spin-mediated contributions to the photocurrents. Such distinction is obtained by analyzing the dependence of the symmetry-breaking induced (transverse) components of the photocurrents on the linear polarization angle of the laser pulse. This suggests a possibility of inferring spin-mediated processes in photocurrents without the use of circularly polarized lights. Moreover, the interplay between transient symmetry breaking and the anisotropy of the Rashba SOC also leads to transiently nonzero spin polarization components that are otherwise zero in the steady-state limit and the linear response regime. Especially, the out-of-plane spin polarization component can be induced or turned off by controlling the relative orientation of the linear polarization with respect to the symmetry axis of the 2D electronic system, without involving material-intrinsic magnetization effects. Our findings demonstrate the efficacy of a particular coordination between the polarization of the ultrafast laser pulses and the spatial symmetry of the electronic materials in directing the real-time charge and the spin responses that are fundamental to the development of ultrafast spintronics in solid states.

I. INTRODUCTION

Revealing and controlling spin-mediated electronic processes via laser-induced excitations constitute a substantial part of the broad research field of solid-state spintronics, where spin-orbit coupling (SOC) is commonly known to play a vital role in many circumstances. Along this direction, one important research line that has drawn considerable efforts (both theoretical and experimental) concerns the manifestation of the two-dimensional (2D) topological surface states, which encode the signature spin-momentum locking effects from the underlying SOC, through the helicity-dependencies of the photo-currents in 3D topological insulators [1–9]. Conventionally, continuous irradiation of circularly polarized light is applied to enable the studies of helicity dependence for engaging spin-mediated processes [1–4, 7]. In place of conventional practices, the uses of ultrafast laser fields with circularly

or even just linearly polarized light also lead to intriguing results. It has been experimentally demonstrated that ultrafast laser fields with circular polarization can achieve control of surface currents with near unity fidelity [6] and generate helicity-dependent terahertz emission with tunable polarity [9]. More noticeably, through the time scale separation between pulse-induced in-plane and out-of-plane excitations, laser pulses with linear polarization has been experimentally shown to be useful for revealing the in-plane anisotropy of the studied surfaces as terminations of the bulks as well as the anisotropy inherited to the intrinsic planar structure of materials of only atomic thickness [8, 10]. This is particularly inspiring for spintronics in 2D, since anisotropic responses to externally applied fields incorporating the SOC effects have caught a lot of attention [1, 11–14, 16–18], despite its primary focus on static fields (see, for example, Ref. [18] and references there in). In light of the combined interests of spintronics with ultrafast lasers [6, 8, 9, 19, 20] and the ubiquitous exhibition of anisotropy in 2D systems, here we are motivated to explore the SOC-related anisotropic effects on spin-mediated electronic processes triggered by ultrafast laser fields.

*Electronic address: kerustemiro@gmail.com

For electrons moving in 2D, a widely studied form of SOC is the Rashba SOC [21, 22]. The Rashba SOC in its simplest form, which is linear in k , only produces isotropic spin splitting. It is possible to produce anisotropic spin splitting by involving k -higher-order terms from the special properties of the interfaces [23, 24], or even by periodic modulation from continuous laser irradiation [25]. Nevertheless, from a modeling point of view, there exists a number of straightforward modifications, starting from the elementary Rashba SOC, that produce simple linear-in- k anisotropic spin splittings which underlie the rich results of anisotropic spin-related responses [1, 11–14, 16–18]. The existence of k -linear anisotropic spin splitting is also witnessed in several ab initio studies for a number of different 2D materials hosting Rashba SOC [9, 11, 12]. In terms of modeling, one well-known approach to produce such effect is to include Dresselhaus SOC along with the Rashba SOC [12, 13, 29]. Another widely applied approach goes by adding to the Rashba Hamiltonian a momentum-independent Zeeman-splitting term, whose corresponding magnetic field has non-vanishing in-plane components. This underlies the analysis of anisotropic magnetoresistance effects where the Zeeman field is externally applied [11, 17]. It also captures the notion of Rashba ferromagnets where the Zeeman field describes the effect of the internal magnetization [14, 30–32]. Note that even without considering SOC, anisotropic effects can readily be produced by differences in effective masses along orthogonal directions. Incorporating the Rashba SOC with the underlying physical mechanisms that give rise to anisotropy in the effective masses is yet another route to arrive anisotropic spin splittings [8, 13, 33].

The above different ways of modeling anisotropic spin splittings can be chosen in accordance with different origins of anisotropy that one wishes to address. For definiteness and simplicity, here we only focus on k -linear Rashba models with anisotropic effective masses [1, 13, 16]. Past studies on different aspects of the above setup have hinted further possibilities of unearthing intriguing findings regarding anisotropic spin-mediated responses to external fields. For example, a study on the steady-state current-induced spin polarization (CISP) driven by a static electric field has revealed interesting non-monotonicity in the dependence of spin polarization on the fermi energy. This non-monotonicity behavior is found to be intimately related to the anisotropy which renders the topology of the fermi surfaces being non-trivially fragmented [1]. Another study on the frequency-dependent optical conductivities has shown that with the presence of Rashba SOC, adjusting the ratio between the effective masses can efficiently tune the height and widths of absorption spectra under continuous irradiation [16]. Here we alternatively investigate the transient regime, concentrating on how the spin states and the photocurrents respond to short laser pulses that are expected to reveal the underlying in-plane anisotropy through the dependence on the orientation of linear polarization. Since

prominent anisotropic effects on spin polarization and optical conductivities have been respectively pronounced under static electric fields and time-periodic drivings, one then naturally wonders how the Rashba-SOC-related anisotropy affects the transient responses to pulsed electric fields.

Even without explicating the anisotropic effects, the transient regime itself has been proven to provide valuable insights in the context of Rashba SOC. For instance, a number of studies on CISP (also known as Edelstein effect when the Rashba SOC is addressed [36]) induced by a constant-in-time external electric field have explicitly shown how the steady net spin polarization is determined by the relaxation-time constant whose origin is attributed to extrinsic scattering effects (see Refs. [1, 12, 18, 38], for example). Yet, interestingly, a study on the transient regime with isotropic Rashba SOC and also with a constant-in-time electric field [39] has revealed how the stable CISP can be formed in time, incorporating the full non-perturbation effects of the electric field in the clean limit without extrinsic scattering effects, differentiating itself from previous efforts using linear responses [1, 12, 18, 38]. Furthermore, they found that obviously different magnitudes in the asymptotic spin polarization can be rooted to the differences between the adiabatic and non-adiabatic time-evolution processes. It is natural to ask what happens to the spin polarization associated with the Rashba SOC in real time if one applies a pulsed, instead of a constant-in-time electric field.

Another reason to theoretically investigate the transient dynamics is motivated by an issue called transient symmetry breaking out of purely electronic origin, a term used in Ref.[40] which is an experimental study on Weyl semimetal TaAs illuminated by ultrafast lasers. Crucially, the experimental feasibility of attributing such transient effects to pure electronic origin signifies that the acts of the laser fields on altering the atomic structures (that determine the electronic band structures upon which the calculations of non-equilibrium electronic responses are based) are not significantly relevant. This is indeed a widely employed situation in theoretical studies in which the external fields are only considered to act on the electronic degrees of freedom (see Refs. [1, 16, 18, 39], for example). In the experiment of Ref. [40], through examining the time-dependent patterns of second harmonic generation (SHG) against prescribed symmetry requirements, they established the transient breaking of both time-reversal and spatial symmetries. Compared to real experimental 3D materials, the spatial symmetry of 2D anisotropic Rashba models (with C_{2v} symmetry [1, 8]) is much more simplified. Furthermore, previously mentioned studies have demonstrated the usefulness of ultrafast linear polarized lasers on resolving the 2D anisotropic effects [8, 10]. Given these two observations, in the particular context of anisotropic Rashba SOC, we are then curious about if the inherited anisotropy of C_{2v} symmetry can be used to characterize transient symmetry breaking as an alternative to the analysis of SHG. Further-

more, identifying different physically distinct contributions to the photocurrent, especially differentiating spin-mediated contribution from other contributions, has always been the interests of solid-state opto-spintronics. The information about the roles played by spin in the photocurrent can be extracted from analyzing photocurrents obtained under varying polarization (continuously from linear to circular) of the exciting lasers (see Refs. [2, 6, 9], for example). Here we are wondering how the possible transient-symmetry-breaking effects can cooperate with the effects from anisotropic Rashba SOC to offer a different route of differentiating spin-mediated contribution from other contributions using only linear polarized laser to excite the photocurrents, without involving circular polarization whose effectiveness in probing spin-related aspects of electron transport has been very much explored.

Collecting the above motivations, in this work, we investigate the real-time evolutions of photocurrents and spin polarizations induced by pulsed electric fields with linear polarization in a 2D electron gas with anisotropic Rashba SOC. In Sec. II, we introduce the Hamiltonian for the 2D electron gas with anisotropic Rashba SOC and non-equal effective masses along the two orthogonal crystal axes contained in the two mirror planes of the C_{2v} symmetry. In Sec. III, we explicitly monitor the time evolutions of photocurrents and spin polarizations in three distinct cases, (i): isotropic limit where the two effective masses are equal (ii): the non-isotropic case with the driving field polarized along one of the two crystal axes (iii) the non-isotropic case with the driving field polarized not along any of the two crystal axes (so that the mirror symmetry is broken by the external field). Briefly, we find that when the mirror symmetry is broken by the external field, spin polarization components not present in cases (i) and (ii) can be induced in case (iii) (including non-vanishing out-of-plane spin polarization). In addition, by generically separating the photocurrents into a pure kinetic contribution and a spin-sensitive contribution, we find that through the analysis of the anisotropy of these two contributions' transverse components (flowing in the direction perpendicular to the polarization of external field), the effect of transient symmetry breaking can be exploited to differentiate spin-mediated from charge-mediated processes in the photocurrents. Further implications of our main findings are discussed in Sec. IV.

II. ANISOTROPIC RASHBA SOC, PHOTO-CURRENTS AND SPIN POLARIZATION

A. Anisotropic Rashba SOC

We consider a model of two-dimensional electron gas (2DEG) in the x - y plane, defined by two orthogonal unit vectors \hat{x} and \hat{y} , with anisotropy in the effective masses.

This is described by the Hamiltonian,

$$\mathcal{H}(\mathbf{k}) = \mathcal{H}_K(\mathbf{k}) + \mathcal{H}_{\text{so}}(\mathbf{k}), \quad (1)$$

in which $\mathcal{H}_K(\mathbf{k})$ is the kinetic energy and $\mathcal{H}_{\text{so}}(\mathbf{k})$ describes the SOC. The kinetic energy with anisotropic effective masses is given by

$$\mathcal{H}_K(\mathbf{k}) = \frac{\hbar^2 k_x^2}{2m_x} + \frac{\hbar^2 k_y^2}{2m_y}, \quad (2)$$

where $m_{x/y}$ and $\hbar k_{x/y}$ are the effective mass and the x/y -direction component of the momentum $\hbar\mathbf{k} = \hbar(\hat{x}k_x + \hat{y}k_y)$ [13, 16]. In order to factor out the anisotropic effect, we employ the polar coordinate, namely, $\mathbf{k} = k\hat{\mathbf{k}}$ with $\hat{\mathbf{k}} = \hat{x}\cos\theta + \hat{y}\sin\theta$ in which θ is the angle between the momentum $\hbar\mathbf{k}$ and the x -axis and $k = |\mathbf{k}|$. This rewrites Eq. (2) to

$$\mathcal{H}_K(\mathbf{k}) = \frac{\hbar^2 k^2}{2m_r} \mathcal{I}_K(r_A, \theta), \quad (3)$$

where

$$\mathcal{I}_K(r_A, \theta) = \left[\sqrt{r_A} \cos^2\theta + \sqrt{1/r_A} \sin^2\theta \right], \quad (4)$$

with

$$r_A \equiv m_y/m_x. \quad (5)$$

Note that $\mathcal{I}_K(r_A, \theta)$ in Eq. (4) is a dimensionless quantity, independent of k and $m_r = \sqrt{m_x m_y}$ that together determine the magnitude of the kinetic energy for its θ -independent part. When $r_A = 1$, $\mathcal{I}_K(r_A = 1, \theta) = 1$ becomes independent θ and we are back to the isotropic limit. The deviation of r_A from unity is thus reflected by the non-vanishing variation of $\mathcal{I}_K(r_A, \theta)$ with respect to θ , characterizing the anisotropy, namely, the dependence on θ .

The Rashba SOC is induced by the asymmetry in the out-of-plane direction \hat{z} [21], namely, $H_{\text{so}} \propto \boldsymbol{\sigma} \cdot (\mathbf{v} \times \hat{z})$, where $\boldsymbol{\sigma}$ is the three-component vector of Pauli matrices for the spin and $\mathbf{v} = \hbar^{-1} \partial \mathcal{H}_K / \partial \mathbf{k}$ is the electron velocity. The anisotropy in the effective masses thus results in the Rashba SOC as

$$\mathcal{H}_{\text{so}}(\mathbf{k}) = \boldsymbol{\Omega}(\mathbf{k}) \cdot \boldsymbol{\sigma}, \quad (6)$$

where

$$\boldsymbol{\Omega}(\mathbf{k}) = \alpha_R [\mathcal{X}_K(r_A) \mathbf{k}] \times \hat{z}, \quad (7)$$

is called the spin-orbit field [29] with α_R the Rashba coefficient and

$$\mathcal{X}_K(r_A) = \begin{pmatrix} r_X^K & 0 \\ 0 & r_Y^K \end{pmatrix}, \quad (8)$$

anisotropically rescales the components k_x and k_y of the vector $\mathbf{k} = k_x \hat{x} + k_y \hat{y}$ to $\mathcal{X}_K(r_A) \mathbf{k} = r_X^K k_x \hat{x} + r_Y^K k_y \hat{y}$ with $r_X^K = \sqrt{m_y/m_x}$ and $r_Y^K = \sqrt{m_x/m_y}$. By setting

$r_A = 1$, Eq. (6) reduces to the familiar isotropic Rashba SOC with $\mathbf{\Omega}(\mathbf{k}) = \alpha_R \mathbf{k} \times \hat{z}$. The Rashba SOC induces a spin splitting which gives rise to the dispersion relation

$$\varepsilon_{\pm}(\mathbf{k}) = \frac{\hbar^2 k^2}{2m_r} \mathcal{I}_K(r_A, \theta) \pm k \alpha_R \mathcal{I}_{SO}(r_A, \theta), \quad (9)$$

where

$$\mathcal{I}_{SO}(r_A, \theta) = \sqrt{r_A \cos^2 \theta + r_A^{-1} \sin^2 \theta}, \quad (10)$$

also dimensionless, explicitly depicts the anisotropy of the spin splitting through $\partial \mathcal{I}_{SO}(r_A \neq 1, \theta) / \partial \theta \neq 0$.

Despite the breaking of isotropy by $r_A \neq 1$, the Hamiltonian Eq. (1) well exhibits the time-reversal symmetry (TRS) and the C_{2v} symmetry [1]. The x - and y -axes along which the effective masses are defined naturally give the two mirror planes, namely, the x - z mirror plane M_{xz} and the y - z mirror plane M_{yz} . For simplicity, here we call the x - and y -axes as the mirror lines. These symmetries are inherited to the equilibrium properties before the external field is turned on to push the electron gas out of equilibrium. The equilibrium properties for such systems with SOC can be characterized by its spin texture that we now define. We assume that at equilibrium specified by the fermi energy ε_F (at zero temperature), we are in the low-energy regime where only the lower band is occupied (see details of the fermi surface in Sec. A of Ref. [41]). We denote by $|u_n(\mathbf{k})\rangle$ the wavefunction for band n satisfying $\mathcal{H}(\mathbf{k})|u_n(\mathbf{k})\rangle = \varepsilon_n(\mathbf{k})|u_n(\mathbf{k})\rangle$ and $\varepsilon_n(\mathbf{k})$ with $n = \pm$ given in Eq. (9). The equilibrium spin texture is the spin expectation value as a function of \mathbf{k} for the occupied band, namely, $\langle \boldsymbol{\sigma} \rangle_{\text{eq}}(\mathbf{k}) = \langle u_-(\mathbf{k}) | \boldsymbol{\sigma} | u_-(\mathbf{k}) \rangle$ with a corresponding net spin polarization, $\mathbf{S}_{\text{eq}} = (\hbar/2) \int d^2 \mathbf{k} \langle \boldsymbol{\sigma} \rangle_{\text{eq}}(\mathbf{k})$. To highlight the role of TRS, we define $\overline{\langle \boldsymbol{\sigma} \rangle}_{\text{eq}}(\mathbf{k}) = \langle \boldsymbol{\sigma} \rangle_{\text{eq}}(\mathbf{k}) + \langle \boldsymbol{\sigma} \rangle_{\text{eq}}(-\mathbf{k})$ and rewrite

$$\mathbf{S}_{\text{eq}} = \frac{\hbar}{2} \int_{\text{half S.F.}} d^2 \mathbf{k} \overline{\langle \boldsymbol{\sigma} \rangle}_{\text{eq}}(\mathbf{k}), \quad (11)$$

where in $\int_{\text{half S.F.}} d^2 \mathbf{k}$ the integration is only over half of the fermi surface. Obviously from Eq. (6), one has $\langle \boldsymbol{\sigma} \rangle_{\text{eq}}(\mathbf{k}) = -\mathbf{\Omega}(\mathbf{k}) / |\mathbf{\Omega}(\mathbf{k})|$ with $\mathbf{\Omega}(\mathbf{k}) = -\mathbf{\Omega}(-\mathbf{k})$ showing the TRS. We then see that the TRS dictates $\overline{\langle \boldsymbol{\sigma} \rangle}_{\text{eq}}(\mathbf{k}) = 0$ and therefore $\mathbf{S}_{\text{eq}} = 0$. The out-of-plane spin at equilibrium is zero, $\hat{z} \cdot \langle \boldsymbol{\sigma} \rangle_{\text{eq}}(\mathbf{k}) = 0$ since the spin-orbit field $\mathbf{\Omega}(\mathbf{k})$ only lies on the x - y plane. Typical equilibrium spin textures for isotropic and anisotropic Rashba SOC systems are schematically presented in Fig. 1 in accordance with Eq. (A5) and $\langle \boldsymbol{\sigma} \rangle_{\text{eq}}(\mathbf{k}) = -\mathbf{\Omega}(\mathbf{k}) / |\mathbf{\Omega}(\mathbf{k})|$.

B. Real-time photocurrents and spin polarization

With the equilibrium properties in mind, next we want to study the non-equilibrium states induced by pulsed

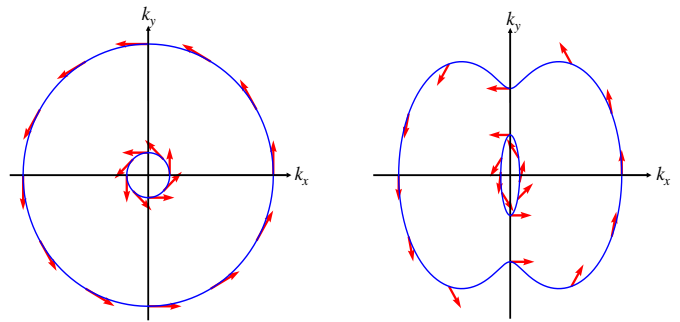


Figure 1: Schematic illustrations of equilibrium spin textures for isotropic (left panel) ($r_A = 1.0$) and anisotropic (right panel) ($r_A = 3.0$) Rashba SOC. Both are with $\varepsilon_F = -0.5\varepsilon_{\text{so}}^*$. The blue lines mark the fermi contours and the red arrows mark the spin.

electric fields that cause time-dependent photocurrents and spin polarizations. Here we adopt a wave-packet picture for formulating the spin polarization and photocurrent of an electron gas. The description starts from a single-electron wave packet and treats the electron gas as an ensemble of wave packets [2, 3].

When one applies an electric field $\mathbf{E}(t)$, an electron wave packet that initially carries momentum \mathbf{k} will be pushed to a state with momentum \mathbf{k}_t , found by

$$\dot{\mathbf{k}}_t = -(\varepsilon/\hbar) \mathbf{E}(t), \quad (12)$$

with the initial condition $\mathbf{k}_{t=t_0} = \mathbf{k}$ where t_0 denotes the initial time before which the electron gas is at equilibrium. The solution to Eq. (12) is $\mathbf{k}_t = \mathbf{k} + \mathcal{K}_t$, where $\mathcal{K}_t = (-\varepsilon/\hbar) \int_{t_0}^t dt' \mathbf{E}(t')$ stands for the momentum transferred to the carrier by the electric field. By averaging over the ensemble of wave packets, the state of the electron gas at time t is specified by the (one-body) density matrix $\varrho_{\mathbf{k}}(t)$. At $t = t_0$, it is given by $\varrho_{\mathbf{k}}(t_0) = \varrho_{\mathbf{k}}^{\text{eq}}$, where

$$\varrho_{\mathbf{k}}^{\text{eq}} = \sum_n f^0(\varepsilon_n(\mathbf{k})) |u_n(\mathbf{k})\rangle \langle u_n(\mathbf{k})|, \quad (13)$$

in which $|u_n(\mathbf{k})\rangle$ satisfies $\mathcal{H}(\mathbf{k})|u_n(\mathbf{k})\rangle = \varepsilon_n(\mathbf{k})|u_n(\mathbf{k})\rangle$ with $\varepsilon_n(\mathbf{k})$ the band energy and the equilibrium fermi distribution function is

$$f^0(\varepsilon) = \frac{1}{e^{(\varepsilon - \varepsilon_F)/k_B T} + 1}. \quad (14)$$

Respectively, ε_F and T are the equilibrium fermi energy and temperature. Below we specify the density matrix for circumstances of interests.

1. the ideal electron gas

If we assume that we have an electron gas lacking of any scattering mechanism (a situation termed ideal electron gas throughout this work), then for a single wave

packet starting from momentum \mathbf{k} , its state at time t is then governed by the Schrödinger equation

$$\mathcal{H}(\mathbf{k}_t) |u(t)\rangle = i\hbar |\dot{u}(t)\rangle, \quad (15)$$

which has the formal solution $|u(t)\rangle = U_{\mathbf{k}}(t, t_0) |u(t_0)\rangle$ where the evolution operator reads

$$U_{\mathbf{k}}(t, t_0) = \hat{T} \exp \left\{ -\frac{i}{\hbar} \int_{t_0}^t dt' \mathcal{H}(\mathbf{k}_{t'}) \right\} \quad (16)$$

with \hat{T} the time-ordering operator. For an ensemble of such wave packets, the non-equilibrium density matrix at time $t > t_0$ is simply given by

$$\varrho_{\mathbf{k}}^{\text{id}}(t) = U_{\mathbf{k}}(t, t_0) \varrho_{\mathbf{k}}(t_0) U_{\mathbf{k}}(t_0, t), \quad (17)$$

where we have used $U_{\mathbf{k}}(t_0, t) = U_{\mathbf{k}}^\dagger(t, t_0)$ and the superscript id designates the ideal electron gas. The time-dependent photocurrent and spin polarization can then be computed from Eq. (17) (see later discussions around Eqs. (21) and (24)).

2. non-ideal situations

In the non-ideal situations, the scattering and the noises experienced by the wave packet can lead to relaxation and decoherence. In the standard treatment exemplified by Refs. [2, 3], these non-ideal effects have been taken into account along with adiabatic approximation on Eq. (15) (in which the wave packet sticks to one band). With additional inclusion of interband transition up to the first order of the driving electric field (linear response), successful manifestations of Berry curvature effects on wave packet transport have been extensively explored Ref. [3, 44, 45]. For the interests of ultrafast photocurrent responses, the applied electric fields vary rapidly in time with large peak values (for example, 1V/nm [46]). This then calls for a treatment beyond linear response and adiabatic approximation. With static electric fields of intermediate strengths that can break the validity of adiabatic approximations in materials with narrow gaps, a non-adiabatic generalization of Refs. [2, 3] has been developed in Ref. [4] and applied to study the non-adiabatic aspects of valley Hall conduction [48] along with its implications on the non-Abelian characters associated multiple-band effects [49]. With a straightforward extension of Ref. [4] from static electric fields to time-dependent drivings (see details in Sec. B of Ref. [41]), we arrive in

$$\varrho_{\mathbf{k}}(t) = \bar{\varrho}_{\mathbf{k}}(t) + \delta\varrho_{\mathbf{k}}(t), \quad (18a)$$

where

$$\bar{\varrho}_{\mathbf{k}}(t) = \sum_i g_i^0(\mathbf{k}_t) |u_i(\mathbf{k}_t)\rangle \langle u_i(\mathbf{k}_t)|, \quad (18b)$$

and

$$\delta\varrho_{\mathbf{k}}(t) = - \int_{t_0}^t dt' P(t, t') \frac{\partial}{\partial t'} \bar{\varrho}_{\mathbf{k}}^U(t, t'), \quad (18c)$$

in which

$$\bar{\varrho}_{\mathbf{k}}^U(t, t') = U_{\mathbf{k}}(t, t') \bar{\varrho}_{\mathbf{k}}(t') U_{\mathbf{k}}(t', t). \quad (18d)$$

Here $|u_i(\mathbf{k}_t)\rangle$ is the i th hybridized band wavefunction, namely, $\bar{\mathcal{H}}(\mathbf{k}_t, \mathbf{E}(t)) |u_i(\mathbf{k}_t)\rangle = \mathcal{E}_i(\mathbf{k}_t) |u_i(\mathbf{k}_t)\rangle$, where the field-induced band hybridization is captured by the moving-frame Hamiltonian given by $\bar{\mathcal{H}}_{n,m}(\mathbf{k}_t, \mathbf{E}(t)) = \delta_{n,m} \varepsilon_n(\mathbf{k}_t) + (1 - \delta_{n,m}) \bar{\mathcal{R}}_{n,m}(\mathbf{k}_t) \cdot e\mathbf{E}(t)$ in which $\bar{\mathcal{R}}_{n,m}(\mathbf{k}_t) = e^{-i\gamma_n(\mathbf{k}_t)} \mathcal{R}_{n,m}(\mathbf{k}_t) e^{i\gamma_m(\mathbf{k}_t)}$ with $\mathcal{R}_{n,m}(\mathbf{k}_t) = i \langle u_n(\mathbf{k}_t) | (\partial/\partial \mathbf{k}_t) | u_m(\mathbf{k}_t) \rangle$ and $\gamma_n(\mathbf{k}_t) = \int_{\mathbf{k}_{t_0}}^{\mathbf{k}_t} d\mathbf{k}' \cdot \mathcal{R}_{n,n}(\mathbf{k}')$ the Berry connection and Berry phase respectively [4, 48]. $\mathcal{E}_i(\mathbf{k}_t)$ is the hybridized band energy, $g_i^0(\mathbf{k}_t) = f^0(\mathcal{E}_i(\mathbf{k}_t))$ and $P(t, t') = \exp \left[- \int_{t'}^t dt'' \tau_{\mathbf{k}_{t''}}^{-1} \right]$ is the probability for the wave packet to evolve in a scattering-free manner during the time interval $[t', t]$ in which $\tau_{\mathbf{k}}^{-1}$ is the scattering rate for a wave packet carrying momentum \mathbf{k} . More details can be found in the supplementary [41] along with reproductions of some widely applied linear and nonlinear response results by taking the corresponding limits.

We assume that $\mathbf{E}(t \leq t_0) = 0$ and the non-equilibrium process starts for $t > t_0$. At $t = t_0$, we then have $\delta\varrho_{\mathbf{k}}(t_0) = 0$ and $\bar{\varrho}_{\mathbf{k}}(t_0) = \varrho_{\mathbf{k}}^{\text{eq}}$ in Eq. (18) since there is not yet field-induced hybridization of bands, ensuring the initial equilibrium state $\varrho_{\mathbf{k}}(t_0) = \varrho_{\mathbf{k}}^{\text{eq}}$. One can rewrite Eq. (18) via integration-by-part to $\varrho_{\mathbf{k}}(t) = \bar{\varrho}_{\mathbf{k}}^U(t, t_0) P(t, t_0) + \int_{t_0}^t dt' \bar{\varrho}_{\mathbf{k}}^U(t, t') P(t, t') / \tau_{\mathbf{k}_{t'}}$. If we let $\tau_{\mathbf{k}} \rightarrow \infty$, then $\int_{t_0}^t dt' \bar{\varrho}_{\mathbf{k}}^U(t, t') P(t, t') / \tau_{\mathbf{k}_{t'}} \rightarrow 0$, $P(t, t_0) \rightarrow 1$, and by the use of $\bar{\varrho}_{\mathbf{k}}(t_0) = \varrho_{\mathbf{k}}^{\text{eq}}$, we have $\varrho_{\mathbf{k}}(t) \rightarrow \varrho_{\mathbf{k}}^{\text{id}}(t)$. So assuming the relaxation times to be infinite reduces the time-dependent density matrix of Eq. (18) for non-ideal situations to that for an ideal electron gas without any scattering effects of Eq. (17). We now formulate the current and the spin polarization in terms of the density matrix. We will discuss these physical observables calculated from both the density matrix for ideal electron gases and the one including relaxation effects so that we know which effects are intrinsic.

3. Current and spin polarization

The velocity operator of a wave packet of momentum \mathbf{k} is defined by

$$\mathbf{V}(\mathbf{k}) \equiv \frac{\partial \mathcal{H}(\mathbf{k})}{\partial \hbar \mathbf{k}}. \quad (19)$$

For an ensemble of wave packets, the current reads

$$\mathbf{j}(t) = -e \int d^2 \mathbf{k} \text{Tr}(\mathbf{V}(\mathbf{k}_t) \varrho_{\mathbf{k}}(t)), \quad (20)$$

where $-e$ is the charge carried by each of the electron wave packets and note that \mathbf{k}_t in the integrand of Eq. (20) is subject to $\mathbf{k}_{t=t_0} = \mathbf{k}$ which is integrated over. According to Eq. (1), $\mathcal{H}(\mathbf{k}) = \mathcal{H}_K(\mathbf{k}) + \mathcal{H}_{so}(\mathbf{k})$, the current can then be split into two contributions, namely,

$$\mathbf{j}(t) = \mathbf{j}_K(t) + \mathbf{j}_{so}(t), \quad (21a)$$

where

$$\mathbf{j}_K(t) = -e \int d^2\mathbf{k} \text{tr} \left(\rho_{\mathbf{k}}(t) \frac{\partial H_K(\mathbf{k}_t)}{\partial \hbar \mathbf{k}_t} \right), \quad (21b)$$

$$\mathbf{j}_{so}(t) = -e \int d^2\mathbf{k} \text{tr} \left(\rho_{\mathbf{k}}(t) \frac{\partial H_{so}(\mathbf{k}_t)}{\partial \hbar \mathbf{k}_t} \right). \quad (21c)$$

Explicitly, using Eq. (1), we have

$$\mathbf{j}_K(t) = -e \mathcal{X}_K \int d^2\mathbf{k} N_{\mathbf{k}}(t) \frac{\hbar \mathbf{k}_t}{m_r}, \quad (22)$$

$$\mathbf{j}_{so}(t) = \left(\frac{-e}{\hbar/2} \right) \frac{\alpha_R}{\hbar} \hat{\mathbf{z}} \times \mathcal{X}_S \mathbf{S}(t), \quad (23)$$

where $N_{\mathbf{k}}(t) = \text{tr}(\rho_{\mathbf{k}}(t))$ is the occupation for the bands at momentum \mathbf{k}_t and

$$\mathbf{S}(t) = \frac{\hbar}{2} \int d^2\mathbf{k} \langle \boldsymbol{\sigma} \rangle(\mathbf{k}, t), \quad (24)$$

is the net spin polarization of the electron gas obtained by collecting the spin expectation values, $\langle \boldsymbol{\sigma} \rangle(\mathbf{k}, t) \equiv \text{Tr}(\boldsymbol{\sigma} \rho_{\mathbf{k}}(t))$, of all the electron wave packets. The quantity in Eq. (24) has the dimension of angular momentum per unit area as spin density. Here \mathcal{X}_K is the anisotropic scaling tensor introduced in Eq. (8) and

$$\mathcal{X}_S = \begin{pmatrix} r_Y^K & 0 \\ 0 & r_X^K \end{pmatrix}, \quad (25)$$

is formed by swapping the diagonals of \mathcal{X}_K . The contribution, $\mathbf{j}_K(t)$, purely comes from kinetic energy $\mathcal{H}_K(\mathbf{k})$ and is attributed to charge-mediated processes which readily exist without evoking spins. In contrast, $\mathbf{j}_{so}(t)$, as shown by Eqs. (23) and (24) sensitively depends on carrier spins. By comparing Eq. (24) with Eq. (11), one finds that $\langle \boldsymbol{\sigma} \rangle(\mathbf{k}, t_0) = \langle \boldsymbol{\sigma} \rangle_{\text{eq}}(\mathbf{k})$ and $\mathbf{S}(t_0) = \mathbf{S}_{\text{eq}} = 0$. For $t > t_0$, as the external field drives the system out of equilibrium, $\langle \boldsymbol{\sigma} \rangle(\mathbf{k}, t)$ in Eq. (24) naturally stands for the non-equilibrium counterpart of the spin texture, which is responsible for expected nonzero values of induced spin polarization that is also coupled to the spin-sensitive part of the photo-current, $\mathbf{j}_{so}(t)$. Note that one does not expect the ideal electron gas to reach a zero-current state even long after the electric-field pulse is switched off simply because the energy absorbed from the driving field by an ideal electron gas cannot be relaxed by definition. With the relaxation effects taken into account, Eq. (18)

with Eqs. (21) and (24) ensure that the photo-excited currents as well as spin polarizations will eventually decay to zero after the electric field is switched off [50].

Equipped with Eqs. (22), (23) and (24), we are now ready to explore real-time properties of laser-induced photocurrents and spin polarizations. To simplify the discussion of the anisotropic effects, here we exclusively consider only linear polarization, namely, $\mathbf{E}(t) = \hat{\mathbf{e}}E(t)$ with $\hat{\mathbf{e}} \cdot \hat{\mathbf{e}} = 1$ and the orientation of the applied field, $\hat{\mathbf{e}} = \hat{\mathbf{x}} \cos \varphi_e + \hat{\mathbf{y}} \sin \varphi_e$, specified by an angle $0 \leq \varphi_e \leq \pi$, is constant in time. The effects of the anisotropy can then be revealed through the dependence on the orientation φ_e of the applied electric field. We denote $S^{\parallel}(t) = \hat{\mathbf{e}} \cdot \mathbf{S}(t)$ and $S^{\perp}(t) = (\hat{\mathbf{z}} \times \hat{\mathbf{e}}) \cdot \mathbf{S}(t)$ and the same notational convention is applied to other vectorial quantities.

III. SPECIAL NON-EQUILIBRIUM SPIN POLARIZATION INDUCED BY ANISOTROPIC RASHBA SOC

Before we start investigating pulse-triggered transient dynamics, we recall two known results from the linear response regime under static electric fields, relevant for our further discussions. First, the applied electric field can induce a nonzero in-plane spin polarization $\mathbf{S} \neq 0$ through the Rashba SOC, known as the Edelstein effect [36]. It is subject to the condition $\mathbf{S} \cdot \mathbf{E} = 0$ regardless the Rashba SOC is isotropic or anisotropic, due to symmetry constraint from the Hamiltonian of Eq. (1) [1]. Second, although the equilibrium spin texture $\langle \boldsymbol{\sigma} \rangle(\mathbf{k}, t_0) = -\boldsymbol{\Omega}(\mathbf{k})/|\boldsymbol{\Omega}(\mathbf{k})|$ is only in-plane (see Eq. (7) where $\hat{\mathbf{z}} \cdot \boldsymbol{\Omega}(\mathbf{k}) = 0$), a driving field under the adiabatic condition is sufficient to induce a nonzero out-of-plane spin texture $\langle \sigma_z \rangle(\mathbf{k}, t > t_0) \neq 0$ but with vanishing net out-of-plane polarization, $\mathbf{S} \cdot \hat{\mathbf{z}} = 0$, that serves the basis of the so-called universal intrinsic spin Hall current studied in Ref. [51] (see a reproduction [52]). Adding a z -component to the Rashba spin-orbit field $\boldsymbol{\Omega}(\mathbf{k})$ of Eq. (7) not only results in nonzero out-of-plane spin polarization due to the out-of-equilibrium effects, but also gives rise to an equilibrium contribution to the spin polarization, rooted exclusively to the nonzero Berry curvature [53].

In the present study with Eq. (1), the Berry curvature is zero [54]. We will show that by going beyond the linear response regime together with anisotropic Rashba SOC, transient spin polarization can be induced to yield $\mathbf{S}(t) \cdot \hat{\mathbf{z}} \neq 0$ and $\mathbf{S}(t) \cdot \mathbf{E} \neq 0$. We will concomitantly study the photocurrents. Comprehending the results of photocurrents and spin polarization will uncover that the transient breaking of the mirror symmetry not only is at play of inducing spin polarization surpassing the above mentioned restrictions but also provides a way to identify spin-mediated processes by distinguishing the spin-sensitive part $\mathbf{j}_{so}(t)$ from the pure kinetic part $\mathbf{j}_K(t)$ of the photocurrent through anisotropic properties.

Note that in Eq. (24), the time-dependent spin polar-

ization is the \mathbf{k} -integration of the transient spin texture $\langle \boldsymbol{\sigma} \rangle(\mathbf{k}, t)$. As we are motivated to understand the possible consequences of field-induced symmetry breaking on both the photocurrent and the spin polarization, it is instructive to also approach the same issue from the symmetry properties of the \mathbf{k} -resolved transient spin texture. Below we first discuss \mathbf{k} -resolved transient spin texture in Sec. III A and after that we will focus on \mathbf{k} -integrated observables in the remaining parts of Sec. III.

A. Transient spin texture

For an ideal electron gas, in which a single electron wave packet is subject to Eq. (15), the time-dependent spin texture is governed by

$$\frac{\hbar}{2} \frac{d \langle \boldsymbol{\sigma} \rangle(\mathbf{k}, t)}{dt} = \boldsymbol{\Omega}(\mathbf{k}_t) \times \langle \boldsymbol{\sigma} \rangle(\mathbf{k}, t). \quad (26)$$

Here the spin-orbit field $\boldsymbol{\Omega}(\mathbf{k}_t)$ acts as a time-dependent effective magnetic field. In analogy to expressing the spin polarization of the equilibrium spin texture as Eq. (11) in terms of $\overline{\langle \boldsymbol{\sigma} \rangle}_{\text{eq}}(\mathbf{k})$, summing up TRS-paired momenta, the non-equilibrium spin polarization is then given by

$$\mathbf{S}(t) = \frac{\hbar}{2} \int_{\text{half S.F.}} d^2 \mathbf{k} \overline{\langle \boldsymbol{\sigma} \rangle}(\mathbf{k}, t), \quad (27)$$

where

$$\overline{\langle \boldsymbol{\sigma} \rangle}(\mathbf{k}, t) = \langle \boldsymbol{\sigma} \rangle(\mathbf{k}, t) + \langle \boldsymbol{\sigma} \rangle(-\mathbf{k}, t) \quad (28)$$

The time evolution of the spin texture from the moment t to the next instant $t + \delta t$ can be found by using the standard fourth order Runge-Kutta method to iterate Eq. (26) with sufficient small δt . The first small time step away from the equilibrium readily contains interesting information about the non-equilibrium spin texture. At time $t = t_1 = t_0 + \delta t$, we have

$$\overline{\langle \sigma_{\perp} \rangle}(\mathbf{k}, t_1) = \overline{\delta s_{\perp}} \mathcal{G}_0(\theta, \varphi_e), \quad (29)$$

$$\overline{\langle \sigma_{\parallel} \rangle}(\mathbf{k}, t_1) = \overline{\delta s_{\parallel}} \mathcal{G}_1(\sqrt{r_A}, \theta, \varphi_e), \quad (30)$$

and

$$\overline{\langle \sigma_z \rangle}(\mathbf{k}, t_1) = \overline{\delta s_z} \mathcal{G}_1(r_A, \theta, \varphi_e), \quad (31)$$

where $\overline{\delta s_{\perp}} = -(2/3)(\alpha_R^2 \mathcal{K}_{t_{1/2}} k)(\delta t/\hbar)^2$ and $\overline{\delta s_z} = -(1/3)[\alpha_R^3 \mathcal{K}_{t_{1/2}}(\mathcal{K}_{t_1} + \mathcal{K}_{t_{1/2}})k](\delta t/\hbar)^3$ are dimensionless amplitudes independent of θ and φ_e in which $\mathcal{K}_t = (-e/\hbar) \int_{t_0}^t dt' E(t')$ is the amount of momentum transfer from the driving field to the electron along the direction $\hat{\mathbf{e}}$ and $t_{1/2} = t_0 + \delta t/2$. The dependencies on θ and φ_e are described by

$$\mathcal{G}_0(\theta, \varphi_e) = 2 \times \frac{\bar{r}(\cos[2(\theta - \varphi_e)] - 1) + \delta r(\cos(2\theta) - \cos(2\varphi_e))}{\sqrt{r_A \cos^2 \theta + r_A^{-1} \sin^2 \theta}}, \quad (32)$$

and

$$\mathcal{G}_1(x, \theta, \varphi_e) = \frac{-(x + x^{-1}) \sin[2(\theta - \varphi_e)] + (x - x^{-1}) [\sin(2\varphi_e) - \sin(2\theta)]}{\sqrt{r_A \cos^2 \theta + r_A^{-1} \sin^2 \theta}}, \quad (33)$$

where $\bar{r} \equiv (r_Y^K + r_X^K)/2$ and

$$\delta r \equiv \frac{(r_Y^K - r_X^K)}{2}, \quad (34)$$

also quantifies the amount of anisotropy in the effective masses, apart from $r_A = m_y/m_x$ already introduced in Eq. (5) (recall that $r_X^K = \sqrt{m_y/m_x}$ and $r_Y^K = \sqrt{m_x/m_y}$ are the elements of the tensor of Eq. (8) that anisotropically rescale the Bloch momentum). Note that for the well-known linear Edelstein effect in the steady state [36], as well as the non-perturbation aspects of it during the transients under isotropic Rashba SOC with static fields [39], the primary interests lie on S^{\perp} , the in-plane component of the net spin polarization perpendicular to $\hat{\mathbf{e}}$. The texture behind this component of spin polarization is given by $\overline{\langle \sigma_{\perp} \rangle}(\mathbf{k}, t_1)$ of Eq. (29). It is worth noticing that this component has a dependence on θ and φ_e described by $\mathcal{G}_0(\theta, \varphi_e)$ of Eq. (32) that is distinct from $\mathcal{G}_1(x, \theta, \varphi_e)$ of Eq. (33) shared by the other two components, $\overline{\langle \sigma_{\parallel} \rangle}(\mathbf{k}, t_1)$ (with $x = \sqrt{r_A}$) and $\overline{\langle \sigma_z \rangle}(\mathbf{k}, t_1)$ (with $x = r_A$), perpendicular to $\overline{\langle \sigma_{\perp} \rangle}(\mathbf{k}, t_1)$. Although the components $S^{\parallel}(t)$ and $S^z(t)$ of the net spin polarization are not of main concern in the earlier discussions of the Edelstein effect, here we will show that these components are vital to manifest the main effects of the anisotropy of Rashba SOC. The trends for the responses of these components also distinguish themselves from that of $S^{\perp}(t)$.

Facilitated by Eqs. (29), (30) and (31) with the aids from Eqs. (32) and (33), we are now in a position to explore the meaning of transient symmetry breaking from the view of spin texture. Most apparently, in contrast to the equilibrium spin texture where the TRS is respected by $\overline{\langle \boldsymbol{\sigma} \rangle}_{\text{eq}}(\mathbf{k}) = 0$, breaking of TRS is evidenced by $\overline{\langle \boldsymbol{\sigma} \rangle}(\mathbf{k}, t_1) \neq 0$, which is held for general \mathbf{k} as long as $\mathbf{k} \nparallel \hat{\mathbf{e}}$. For $\mathbf{k} = \pm k \hat{\mathbf{e}} \parallel \hat{\mathbf{e}}$, the direction of the time-dependent spin-orbit field $\boldsymbol{\Omega}(\mathbf{k}_t)$ remains constant in time as $-\hat{\mathbf{z}} \times \mathcal{X}_K \hat{\mathbf{e}}/|\mathcal{X}_K \hat{\mathbf{e}}|$ and only its magnitude $|\boldsymbol{\Omega}(\mathbf{k}_t)| = \alpha_R |\mathcal{K}_t \pm k|$ changes with time in Eq. (26) leading to $\langle \boldsymbol{\sigma} \rangle(\pm k \hat{\mathbf{e}}, t) = \langle \boldsymbol{\sigma} \rangle_{\text{eq}}(\pm k \hat{\mathbf{e}})$ (so that $\overline{\langle \boldsymbol{\sigma} \rangle}(\pm k \hat{\mathbf{e}}, t) = 0$).

In the motivating experiment [40], the effect of transient TRS breaking has been established by showing the necessity for the coefficients describing the SHG angular profile to be complex other than real. Without the involvement of laser fields, an earlier study in pure electronic transport setup as two-terminal nanoscale Aharonov-Bohm interferometers have revealed the transient TRS breaking effectively through the loss of phase rigidity in the charge currents without considering spins

[55]. This also underlies the transient spin-polarized current with zero magnetic flux in a similar setup but including SOC [56]. Here through the analysis of the transient spin texture [57], we found quite generically that under the driving of an external electric field, two electron wave packets starting from time-reversal paired momenta and spins (such that the sum of the spins of the two wave packets is zero), are transiently driven to states whose spin expectation values do not sum up to zero and thus one breaks the TRS. This notion of transient breaking of TRS can thus be straightforwardly understood from the above intuitive picture. Next, we discuss how the transient spin texture embeds the effect of breaking of spatial symmetry by focusing on the isotropic limit where the dispersion displays continuous rotation symmetry around the z -axis.

In the isotropic limit $r_A = 1$, the familiar Edelstein effect in the literature [36, 39] gives $S^\perp \neq 0$ while $S^\parallel = S^z = 0$ for the macroscopic net spin polarization. Here we obtain the same conclusion with additional microscopic insights from the non-equilibrium spin texture. Setting $r_A = 1$ simplifies Eqs. (29), (30) and (31) to

$$\overline{\langle \sigma_\perp \rangle}(\mathbf{k}, t_1) = 2\overline{\delta s_{//}} [\cos(2\theta - 2\varphi_e) - 1], \quad (35)$$

$$\overline{\langle \sigma_\parallel \rangle}(\mathbf{k}, t_1) = -2\overline{\delta s_{//}} \sin(2\theta - 2\varphi_e), \quad (36)$$

and

$$\overline{\langle \sigma_z \rangle}(\mathbf{k}, t_1) = -2\overline{\delta s_z} \sin(2\theta - 2\varphi_e), \quad (37)$$

By $\int_0^\pi d\theta \sin(2\theta - 2\varphi_e) = \int_0^\pi d\theta \cos(2\theta - 2\varphi_e) = 0$, we see that $S^\parallel(t_1) = S^z(t_1) = 0$. The nonzero value of $S^\perp(t_1)$ is only due to the θ -independent term in Eq. (35) which is also φ_e -independent. The magnitude of $S^\perp(t_1)$ therefore does not depend on φ_e , as expected by the isotropic condition $r_A = 1$.

Noticeably in the transient spin texture of Eq. (35), $|\overline{\langle \sigma_\perp \rangle}(\mathbf{k}, t_1)|$ becomes larger when θ gets away from φ_e and it is maximized at $\theta = \varphi_e \pm \pi/2$. Furthermore, the mechanism for the vanishing of the spin polarization components orthogonal to S^\perp in the transient process is unlike the mechanism for the vanishing of the net spin polarization at equilibrium $\mathbf{S}_{\text{eq}} = 0$. With the equilibrium spin texture, $\mathbf{S}_{\text{eq}} = 0$ is realized by $\overline{\langle \sigma \rangle}_{\text{eq}}(\mathbf{k}) = 0$, respecting the TRS. In the transient process where the TRS is broken with $\overline{\langle \sigma \rangle}(\mathbf{k}, t_1) \neq 0$, the vanishing of the spin polarization components, $S^\parallel(t_1) = S^z(t_1) = 0$, is realized by the anti-symmetric θ -dependence of the responsible spin texture with respect to $\theta = \varphi_r$, where φ_r specifies the direction of the unit vector $\hat{\mathbf{r}}_S$ given by $\hat{\mathbf{r}}_S \parallel \hat{\mathbf{e}}$ or $\hat{\mathbf{r}}_S \parallel R_{\pi/2}\hat{\mathbf{e}}$ in which $R_{\pi/2}$ is a rotation by $\pi/2$. Explicitly, this means that $\overline{\langle \sigma_{//z} \rangle}(\mathbf{k}, t_1) \Big|_{\theta=\varphi_r+\delta\theta} = -\overline{\langle \sigma_{//z} \rangle}(\mathbf{k}, t_1) \Big|_{\theta=\varphi_r-\delta\theta}$ (see Eqs. (36) and (37)), in which $\delta\theta$ is the angle between \mathbf{k} and $\hat{\mathbf{r}}_S$. The above points manifest that the external field along $\hat{\mathbf{e}}$ creates an

anisotropic feature in the transient spin texture despite $r_A = 1$.

Although the above properties are analytically obtained at the time $t = t_1$, they well remain valid beyond $t > t_1$. This is numerically illustrated in Fig. 2 with the application of a typical Gaussian pulse described by $E(t) = -\dot{A}(t)$ with $A(t) = (E_0/\omega) \sin(\omega t) e^{-(t-t_c)^2/\tau_P^2}$ centered at $t = t_c$. The value of t_c is unimportant since time is counted relative to t_c , as origin of the time axis. We set $t_c = 0$. Since the system is characterized by the Rashba energy $\varepsilon_{\text{so}}^* = m_r \alpha_R^2 / (2\hbar^2)$ and the Rashba wave vector $k_{\text{so}}^* = m_r \alpha_R / \hbar^2$, time is measured in unit of $t^* \equiv 2\pi\hbar/\varepsilon_{\text{so}}^*$ and length is measured in unit of $k_{\text{so}}^*{}^{-1}$. Therefore the strength of electric field is measured in unit of $E_0^* = k_{\text{so}}^* \varepsilon_{\text{so}}^* / e$. To start the non-equilibrium transient process, we assume the system stays at equilibrium till $t = t_0 = t_c - 2\tau_P$ (see captions in Fig. 2 for more details). In Fig. 2(a), the transferred momentum \mathcal{K}_t (in unit of k_{so}^*) as a function of time is plotted showing the profile of the pulse. In Fig. 2(b), the black dotted line clearly shows that $\overline{\langle \sigma_\perp \rangle}(\mathbf{k} \parallel \hat{\mathbf{e}}, t)$ remains zero for all time while the maximum attainable peak in $\overline{\langle \sigma_\perp \rangle}(\mathbf{k}, t)$ is demonstrated with $\theta = \varphi_e + \pi/2$ by the red solid line. The anti-symmetry in the spin texture for the vanishing of the spin polarization components $S^\parallel(t) = S^z(t) = 0$ is demonstrated for $\overline{\langle \sigma_z \rangle}(\mathbf{k}, t)$ and $\overline{\langle \sigma_\parallel \rangle}(\mathbf{k}, t)$ respectively in Fig. 2(c) (with $\varphi_r = \varphi_e$) and Fig. 2(d) (with $\varphi_r = \varphi_e + \pi/2$).

B. dynamics of photocurrents and spin polarization under isotropic Rashba SOC

1. Non-adiabatic spin precession and relaxation effects

The pulse profile of the momentum transferred from the external field, \mathcal{K}_t in Fig. 2(a) shows that its magnitude effectively ceases after $t > t_c + 2\tau_P$. Nevertheless, spin precession persists even long after the external electric field goes away. This is displayed by collecting Fig. 2(b),(c) and (d) for all three components of $\overline{\langle \sigma \rangle}(\mathbf{k}, t)$. Although at a time $t \gg \tau_P$, the spin-orbit field $\Omega(\mathbf{k}_t)$ approaches the initial value $\Omega(\mathbf{k})$, since $\lim_{t \gg \tau_P} \mathcal{K}_t = 0$, the spin expectation value, $\langle \sigma \rangle(\mathbf{k}, t)$, at the same time t typically is not aligned with $\Omega(\mathbf{k}_t) = \Omega(\mathbf{k})$, as a non-adiabatic feature of the full solution to Eq. (26). So a persistent precession of the spin around $\Omega(\mathbf{k})$ is expected.

The macroscopic spin polarization and the corresponding photocurrents are plotted in Fig. 3. Noticeably, due to the lack of relaxation, the non-vanishing spin polarization component $S^\perp(t)$ as well as the spin-sensitive part of the photocurrent, $j_{\text{so}}^\parallel(t) \propto S^\perp(t)$ (see Eq. (23) under $r_A = 1$), retain the oscillatory feature previously observed in the underlying spin texture of Fig. 2 (see the black dashed line and red dashed line in Fig. 3(a) and (b) respectively). The inclusion of relaxation then damps the spin precession so that the pulse-induced spin

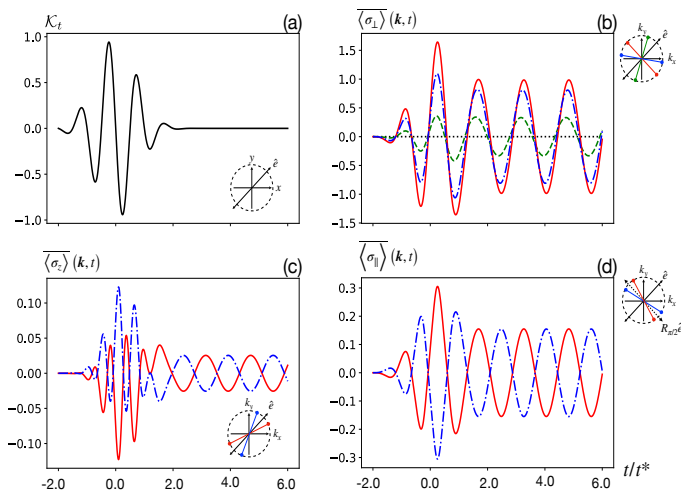


Figure 2: Field-induced anisotropy in the non-equilibrium spin texture under isotropic Rashba SOC. The parameters for the pulse in the numerical demonstrations are chosen to be $\tau_P = t^*$, $\omega = 2\pi/\tau_P$, $E_0 = E_0^*$ with the polarization direction $\varphi_e = 0.25\pi$ (visualized by the inset of plot (a)). The spin texture is examined for $\mathbf{k} = (k, \theta)$ with fixed $k = k_{so}^*$ and various θ 's represented by different curves in plots (b) (as black dotted for $\theta = 0.25\pi$, green dashed for $\theta = 0.4\pi$, red solid for $\theta = 0.75\pi$ and blue dashed for $\theta = 0.95\pi$), (c) (as red solid for $\theta = 0.2\pi$ and blue dashed for $\theta = 0.3\pi$ (so $\delta\theta = 0.05\pi$ with $\varphi_r = 0.25\pi$)) and (d) (as red solid for $\theta = 0.7\pi$ and blue dashed for $\theta = 0.8\pi$ (so $\delta\theta = 0.05\pi$ with $\varphi_r = 0.75\pi$)). The orientations of \mathbf{k} investigated in plots (b),(c) and (d) are visualized respectively in the insets with the corresponding colors.

polarization as well as the spin-sensitive contribution to the photocurrent decays to zero along with the decay of the external field (see the black and the red solid lines in Fig. 3 (a) and (c) respectively). As expected, the amount of the pulse-induced photocurrent in the presence of relaxation effects is smaller than that can be achieved for ideal electron gases (see the obvious difference between the magnitudes of the vertical axis of Fig. 3 (b) (the ideal case) and that of Fig. 3 (c) (including relaxation)).

By comparing the time-dependent profiles of the spin polarization and the photocurrents obtained under the ideal gas assumption with that including relaxation effects (compare the dashed with the solid line in Fig. 3(a), and compare the curve in Fig. 3(b) with that of the same color in Fig. 3(c)), we see that the relaxation effects do not just uniformly damp the magnitudes of these field-induced responses with respect to the ideal case. The peaks of oscillation in the temporal profile of these quantities in the presence of relaxation effects are shifted with respect to those in the absence of scatterings. This reflects the underlying picture, namely, that the coherent propagation of wave packet is disrupted by the presence of scatterings leading to relaxation. Here the relaxation time is assumed to be \mathbf{k} -independent, namely, $\tau_{\mathbf{k}} = \tau$ for all \mathbf{k} 's, so that no anisotropy due to the extrinsic

processes leading to relaxation is included and we can concentrate on the intrinsic anisotropic effects from the effective masses.

2. Spin-sensitive versus kinetic-energy contributions to the photocurrent

With isotropic Rashba SOC, the distinction between the spin-sensitive and the kinetic contributions to the photocurrent is readily visible. In the case of ideal electron gases, while the spin-sensitive part of the photocurrent, $j_{so}^{\parallel}(t)$, shows visible oscillations after the external electric field is effectively off ($t > 2\tau_P$), the pure kinetic contribution to the photocurrent, $j_K^{\parallel}(t)$, smoothly decays to zero, dictated by its being proportional to $\mathcal{K}_t \propto e^{-t^2/\tau_P^2}$ (see the blue dotted line in Fig. 3(b) and the analytical expression for $j_K^{\parallel}(t)$ in Eq. (38) in later discussions). The above is a simple and pedagogical example that illustrates the usefulness of pulse-induced transient responses in differentiating the spin-mediated processes from processes that do not require consideration of spins, for the contributions to the photocurrents.

With or without relaxation effects accounted, $j_{so}^{\parallel}(t)$ differs sharply from $j_K^{\parallel}(t)$ both in terms of the magnitudes and phases of transient oscillations (see the difference between the blue line (for $j_K^{\parallel}(t)$) and the red line (for $j_{so}^{\parallel}(t)$) in both Fig. 3 (b) and (c)). Such visible difference appears not only in the isotropic limit but prevail through all numerical tests in this work (see later discussions). The difference in the overall magnitudes, namely, the peak value reachable in a pulse by $j_K^{\parallel}(t)$ is obviously greater than that by $j_{so}^{\parallel}(t)$, can be explained using Eqs. (22) and (23). In Eq. (22), we see that the magnitude of $j_K^{\parallel}(t)$ is mainly bounded by the amplitude of \mathcal{K}_t as what should be anticipated for an electron gas with usual quadratic dispersion given by \mathcal{H}_K of Eq. (2). In Eq. (23), the magnitude of $j_{so}^{\parallel}(t)$ is determined by that of $S^{\perp}(t)$ whose \mathbf{k} -resolved integrand is subject to $0 \leq |\langle \sigma^{\perp} \rangle(\mathbf{k}, t)|^2 \leq 1$ due to the fundamental bound on the magnitudes of the electron spin. So this quantitative difference actually is rooted to the qualitative difference between how charged particles driven by external electric fields contribute to electric currents and how spin-mediated processes contribute to currents through SOC.

3. implications for anisotropic effects

The above analysis concludes that with isotropic Rashba SOC, the spin polarization is subject to $\mathbf{S}(t) \cdot \hat{\mathbf{z}} = 0$ and $\mathbf{S}(t) \cdot \hat{\mathbf{e}} = 0$. At the same time, we find that the photocurrent has only longitudinal component, namely, $j_K^{\perp}(t) = j_{so}^{\perp}(t) = 0$. These restrictions are held for both ideal calculations without relaxation and the cal-

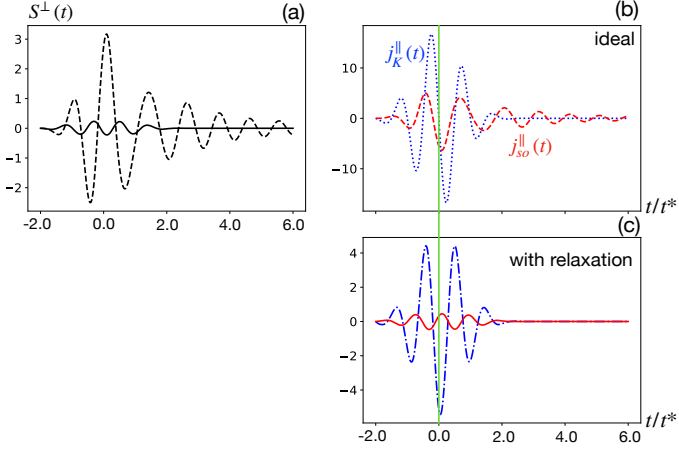


Figure 3: Transient spin polarization (a) (in unit of $(\hbar/2)(k_{\text{so}}^*)^2$ as spin density) and photocurrents ((b) and (c)) (in unit of $-(e/\hbar)k_{\text{so}}^*\varepsilon_{\text{so}}^*$) under isotropic Rashba SOC comparing the ideal electron gas with the one including relaxation effects. The relaxation time demonstrated is $\tau = 0.05t^*$ with other parameters taken from Fig. 2. The equilibrium fermi energy and temperature are $\varepsilon_F = -0.5\varepsilon_{\text{so}}^*$ and $T = 0.01\varepsilon_{\text{so}}^*$. In (a), the black dashed line is for the ideal case and the black solid line includes the relaxation effect. In (b) and (c), the blue dotted and dash-dot lines stand for $j_K^{\parallel}(t)$ respectively in the ideal case and the case with relaxation. The red dashed and solid lines in (b) and (c) are for $j_{\text{so}}^{\parallel}(t)$ computed without and with relaxation effects respectively.

culations with relaxation effect in which the relaxation time is constant for all momenta. Note that the restriction on the spin polarization, namely, $\mathbf{S}(t) \cdot \hat{\mathbf{z}} = 0$ and $\mathbf{S}(t) \cdot \hat{\mathbf{e}} = 0$, and the restriction on the photocurrents, namely, $j_K^{\perp}(t) = j_{\text{so}}^{\perp}(t) = 0$ appear simultaneously. This simultaneous appearance of restrictions on both spin polarization and photocurrents intuitively suggests that if the restriction on the photocurrents $j_K^{\perp}(t) = j_{\text{so}}^{\perp}(t) = 0$ is lift, then it may be possible to also lift the restriction on the spin polarization (and vice versa).

We will soon see that the restriction on $j_K^{\perp}(t) = 0$ can be lift by the anisotropy $m_x \neq m_y$. Since the anisotropy is rooted to $m_x \neq m_y$, its effect is readily manifested in the part of the photocurrent purely due to the kinetic energy. To demonstrate this, we first ignore the scattering effects and $\varrho_{\mathbf{k}}(t)$ is purely given by Eq. (17) as $\varrho_{\mathbf{k}}^{\text{id}}(t)$ and inspects Eq. (22) for $\mathbf{j}_K(t)$. This leads to $\dot{N}_{\mathbf{k}}(t) = \text{tr}(\dot{\varrho}_{\mathbf{k}}^{\text{id}}(t)) = 0$ due to $\dot{\varrho}_{\mathbf{k}}^{\text{id}}(t) = (-i/\hbar)[\mathcal{H}(\mathbf{k}_t), \varrho_{\mathbf{k}}^{\text{id}}(t)]$ and $N_{\mathbf{k}}(t)$ becomes constant in time as $N_{\mathbf{k}}(t) = N_{\mathbf{k}}$. We denote by $\bar{n} = \int d^2\mathbf{k} N_{\mathbf{k}}$ the constant carrier density. By realizing that there is no current at equilibrium, namely, $\mathbf{j}_K(t_0) = 0$, Eq.(22) reduces to $\mathbf{j}_K(t) = -e\bar{n}\frac{\hbar\mathcal{K}_t}{m_r}\mathcal{X}_K\hat{\mathbf{e}}$, or more explicitly,

$$j_K^{\parallel}(t) = -e\bar{n}\frac{\hbar\mathcal{K}_t}{m_r} [r_X^K \cos^2 \varphi_e + r_Y^K \sin^2 \varphi_e], \quad (38)$$

$$j_K^{\perp}(t) = -e\bar{n}\frac{\hbar\mathcal{K}_t}{2m_r} (r_Y^K - r_X^K) \sin(2\varphi_e). \quad (39)$$

The result of Eq.(39) shows that in addition to the anisotropy, $r_X^K \neq r_Y^K$, an extra condition, $\sin(2\varphi_e) \neq 0$, must be satisfied to produce $j_K^{\perp}(t) \neq 0$. This extra condition is satisfied when the external field breaks the mirror symmetry set by the anisotropy, namely, $\hat{\mathbf{e}} \nparallel \hat{\mathbf{x}}$ and $\hat{\mathbf{e}} \nparallel \hat{\mathbf{y}}$ where $\hat{\mathbf{x}}$ and $\hat{\mathbf{y}}$ represent the two mirror lines. Note that Eq.(39) is a transient expression that reflects a well-known fact that when an electric field is applied not along any crystal axis, then a current transverse to it can be generated [59]. This simple expression turns out to be helpful for understanding the effect of transient mirror-symmetry breaking under anisotropic Rashba SOC.

In what follows, we will first discuss the cases where either $\hat{\mathbf{e}} \parallel \hat{\mathbf{x}}$ or $\hat{\mathbf{e}} \parallel \hat{\mathbf{y}}$ is obeyed. Later we will show that indeed, by breaking the mirror symmetry where both $\hat{\mathbf{e}} \nparallel \hat{\mathbf{x}}$ and $\hat{\mathbf{e}} \nparallel \hat{\mathbf{y}}$ are held, the restrictions on the transverse photocurrents together with the that on the spin polarization can be lift away.

C. Anisotropic effects under mirror-symmetry preserving

1. similarity to the isotropic case

Under anisotropic Rashba SOC, namely, $r_A \neq 1$, the Hamiltonian of the system exhibits the mirror symmetry with x - and y -axes being the mirror lines, as mentioned before. By restricting the orientation of the linear polarized external field to $\hat{\mathbf{e}} \parallel \hat{\mathbf{x}}$ or $\hat{\mathbf{e}} \parallel \hat{\mathbf{y}}$, Eqs. (29), (30) and (31) become

$$\overline{\langle \sigma_{\perp} \rangle}(\mathbf{k}, t_1) = -2\overline{\delta s_{//}} \frac{(1 \mp \cos(2\theta))}{\sqrt{(r_X^K \cos \theta)^2 + (r_Y^K \sin \theta)^2}} r_{Y/X}^K, \quad (40)$$

$$\overline{\langle \sigma_{\parallel} \rangle}(\mathbf{k}, t_1) = \mp 2\overline{\delta s_{//}} \frac{\sin(2\theta)}{\sqrt{(r_X^K \cos \theta)^2 + (r_Y^K \sin \theta)^2}} r_{X/Y}^K, \quad (41)$$

and

$$\overline{\langle \sigma_z \rangle}(\mathbf{k}, t_1) = \mp 2\overline{\delta s_z} \frac{\sin(2\theta)}{\sqrt{(r_X^K \cos \theta)^2 + (r_Y^K \sin \theta)^2}} (r_{X/Y}^K)^2, \quad (42)$$

where the upper/lower sign is designated for $\hat{\mathbf{e}} \parallel \hat{\mathbf{x}}/\hat{\mathbf{y}}$. Evidently by Eq. (40), Eqs. (41) and (42), the results obtained under $\hat{\mathbf{e}} \parallel \hat{\mathbf{x}}$ and those obtained under $\hat{\mathbf{e}} \parallel \hat{\mathbf{y}}$ are quantitatively different under $r_X^K \neq r_Y^K$. Nevertheless, the macroscopic net spin polarization with such anisotropy still resembles that obtained under the isotropic condition in the following sense, namely, $S^{\parallel}(t) = S^z(t) = 0$ and the only nonzero component is $S^{\perp}(t)$ (verified through numerical calculations and analytically seen at $t = t_1$ by integrating Eqs. (40), (41)

and (42) over \mathbf{k}). Under the anisotropic Rashba SOC with the restriction $\hat{e} \parallel \hat{\mathbf{x}}$ or $\hat{e} \parallel \hat{\mathbf{y}}$, how the underlying spin texture leads to $S^{\parallel}(t) = S^z(t) = 0$ is quite similar to what has been found for the isotropic condition. The spin textures for these two components are also anti-symmetric with respect to both \hat{e} and $R_{\pi/2}\hat{e}$, as one can read from Eqs. (41) and (42), similar to Eqs. (36) and (37).

This similarity between the results under the isotropic condition and the mirror-symmetry-preserving anisotropic condition is hinted by how the spin polarization and the spin-sensitive part of photocurrent couple to each other, namely, Eq. (23). In the frame spanned by \hat{e} and $\hat{\mathbf{z}} \times \hat{e}$, Eq. (23) becomes

$$\begin{pmatrix} j_{so}^{\parallel}(t) \\ j_{so}^{\perp}(t) \end{pmatrix} = L(r_A, \varphi_e) \begin{pmatrix} S^{\parallel}(t) \\ S^{\perp}(t) \end{pmatrix}, \quad (43a)$$

where $L(r_A, \varphi_e)$ is a 2×2 matrix given by

$$L(r_A, \varphi_e) = \left(\frac{-e}{\hbar/2} \right) \frac{\alpha_R}{\hbar} \times \begin{pmatrix} \sin(2\varphi_e) \delta r & \delta r \cos(2\varphi_e) - \bar{r} \\ \delta r \cos(2\varphi_e) + \bar{r} & -\sin(2\varphi_e) \delta r \end{pmatrix}, \quad (43b)$$

in which the definitions of δr and \bar{r} are found around Eq. (34). Clearly for $\mathbf{S}(t)$ and $\mathbf{j}_{so}(t)$ as \mathbf{k} -integrated quantities, the anisotropy as the dependence on the external field's orientation is reflected on the matrix in Eq. (43) through the φ_e -dependent terms that can only be present when $\delta r \neq 0$. Noticeably, when $\delta r = 0$, $L(r_A, \varphi_e) \propto \begin{pmatrix} 0 & -1 \\ 1 & 0 \end{pmatrix}$ has vanishing diagonals. This structure of the coupling matrix $L(r_A, \varphi_e)$ with zero diagonals is also obtained under $\delta r \neq 0$ when \hat{e} is aligned with either x -axis (in which $2\varphi_e = 0$, or $2\varphi_e = 2\pi$) or y -axis (in which $2\varphi_e = \pi$, or $2\varphi_e = 3\pi$), such that $\sin(2\varphi_e) = 0$. As long as the diagonals of $L(r_A, \varphi_e)$ are zero and $S^{\parallel}(t)$ is zero, then conversely we have $j_{so}^{\perp}(t) = 0$ from Eq. (43). Together with $j_K^{\perp}(t) = 0$ under $\sin(2\varphi_e) = 0$ despite $r_X^K \neq r_Y^K$ as asserted by Eq.(39), the same set of restrictions, $S^{\parallel}(t) = S^z(t) = 0$ and $j_K^{\perp}(t) = j_{so}^{\perp}(t) = 0$, are obtained under anisotropic conditions $r_X^K \neq r_Y^K$ with the external field respecting the mirror symmetry $\hat{e} \parallel \hat{\mathbf{x}}$ or $\hat{e} \parallel \hat{\mathbf{y}}$. This conclusion has been confirmed not only for ideal electron gases but also for the calculations including relaxation effects.

2. difference from the isotropic case

Despite the above mentioned similarity, the presence of anisotropy $r_X^K \neq r_Y^K$ always makes a difference. At least, the magnitudes of the non-vanishing components of the spin polarization and the photocurrent obtained under $\hat{e} \parallel \hat{\mathbf{x}}$ ($\varphi_e = 0$) should be well distinct from that obtained under $\hat{e} \parallel \hat{\mathbf{y}}$ ($\varphi_e = \pi/2$), as demonstrated

in Fig. 4(a) for $\Delta_0 S^{\perp}(t) \equiv S^{\perp}(t)|_{\varphi_e=0} - S^{\perp}(t)|_{\varphi_e=\pi/2}$ and Fig. 4 (b) for $\Delta_0 j^{\parallel}(t) \equiv j^{\parallel}(t)|_{\varphi_e=0} - j^{\parallel}(t)|_{\varphi_e=\pi/2}$ respectively. More than that, for ideal electron gases, in comparison to the isotropic limit where several oscillations in $S^{\perp}(t)$ are visible after $t > 2\tau_P$ where the driving field effectively ceases away, here with the presence of anisotropy, the decay of $S^{\perp}(t)$ after $t > 2\tau_P$ is comparatively significant (compare black dashed line in Fig. 4(a) with that in Fig. 3(a)). This difference can be understood from how integration over \mathbf{k} of the solution to Eq. (26) for an anisotropic fermi surface differs from that for an isotropic fermi surface. In Eq. (26), as t approaches the time where $\Omega(\mathbf{k}_t) \rightarrow \Omega(\mathbf{k})$, the spin precession exhibited as temporal oscillation has its period controlled by $|\Omega(\mathbf{k})|$. For the isotropic case, every angle of \mathbf{k} has the same spin-splitting $\propto |\Omega(\mathbf{k})|$ and the integration over \mathbf{k} 's angles sums over oscillations of the same period $|\Omega(\mathbf{k})|$. The result is then expected to manifest such oscillations. For the anisotropic case, since every angle of \mathbf{k} has different values of $|\Omega(\mathbf{k})|$, summation over oscillations of different periods then smears the effect. With the relaxation effects taken into account, the pulse-induced magnitudes in $\Delta_0 S^{\perp}(t)$ and $\Delta_0 j^{\parallel}(t)$ also become smaller than those obtained under idea gas assumption. This is because the relaxation effects readily reduce the magnitudes of both $S^{\perp}(t)$ and $j^{\parallel}(t)$ obtained under a given φ_e .

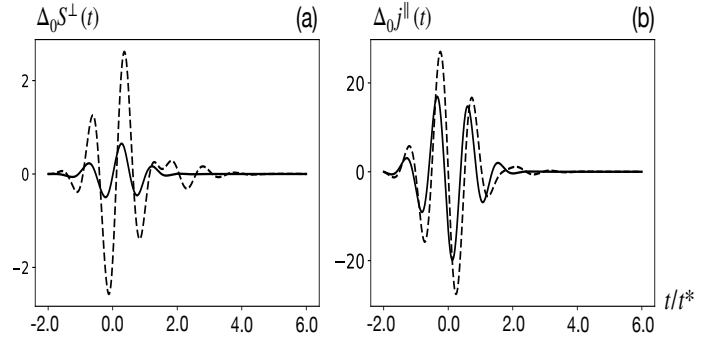


Figure 4: Time dependence of the anisotropy-induced asymmetry in the spin polarization (a) and the photocurrents (b) under mirror-symmetry preserving external fields. The black dashed lines are for ideal electron gases and the black solid lines include relaxation effects ($\tau = 0.2t^*$). Here the anisotropy strength is given by $m_y/m_x = 3$. Other parameters are the same as those used in Fig. 3.

D. Anisotropic effects under mirror-symmetry breaking

The essential effect of the anisotropy in the Rashba SOC, $r_X \neq r_Y$, is largely pronounced when the linear polarization direction is not aligned with either of the two mirror lines, namely, $\hat{e} \nparallel \hat{\mathbf{x}}$ and $\hat{e} \nparallel \hat{\mathbf{y}}$. When this happens, the transverse current from the kinetic energy

becomes nonzero, $j_K^\perp(t) \neq 0$, according to Eq. (39). Concomitantly, as hinted from the simultaneous disappearance of $j^\perp(t)$, $S^\parallel(t)$ and $S^z(t)$ in the previous two cases, namely, the isotropic and mirror-symmetry-preserved anisotropic cases, the spin polarization components, $S^\parallel(t)$ and $S^z(t)$, now gain nonzero values owing to

$$\begin{aligned} & \int_0^\pi d\theta \mathcal{G}_1(x, \theta, \varphi_e) \\ &= \int_0^\pi d\theta \frac{(x+x^{-1})\cos(2\theta) + (x-x^{-1})}{\sqrt{r_A \cos^2\theta + r_A^{-1} \sin^2\theta}} \sin(2\varphi_e) \neq 0, \end{aligned} \quad (44)$$

(see Eqs. (30) and (31) as the underlying spin texture). With $S^\parallel(t) \neq 0$, then through Eq. (43) we also find that $j_{so}^\perp(t) \neq 0$ when the anisotropy-imposed mirror symmetry is broken by $\hat{e} \nparallel \hat{x}$ and $\hat{e} \nparallel \hat{y}$ leading to $\sin(2\varphi_e) \neq 0$.

Interestingly, the factor $\sin(2\varphi_e)$, which we have previously mentioned regarding Eq. (43) for manifesting the anisotropic effect of $\delta r = r_Y^K - r_X^K \neq 0$ in how the spin polarization and the spin-sensitive part of the photocurrent are coupled, appears again simultaneously in Eq.(39) (for $j_K^\perp(t)$) and in Eq. (44) (for $S^\parallel(t_1)$ and $S^z(t_1)$). Here in Eqs. (39) and (44) (both are derived for ideal electron gases) it describes the dependence of these physical observables on the orientation of the applied field φ_e . In addition to being nonzero only when \hat{e} is not parallel to any of the mirror lines, this simple factor $\sin(2\varphi_e)$ also conveys other properties arising from breaking the mirror symmetry. (i): By a mirror reflection upon \hat{e} , namely $\varphi_e \rightarrow \pi - \varphi_e$, the signs of those mirror-symmetry-breaking induced physical responses should also be flipped, inferred from $\sin(2\varphi_e) = -\sin[2(\pi - \varphi_e)]$. (ii) Breaking the mirror symmetry by deviating \hat{e} of a given angle $\delta\varphi$ away from the x -mirror line or from the y -mirror line should not affect the magnitude of the responding physical quantities, inferred from $\sin(2\varphi_e)|_{\varphi_e=\delta\varphi} = \sin(2\varphi_e)|_{\varphi_e=\pi/2-\delta\varphi}$. Below we will show that by investigating the spin polarization and the photocurrents against these two points (i) and (ii), we will be able to contrast physical responses induced by mirror-symmetry breaking with those not arising from this mechanism and distinguish spin-sensitive contributions to the transverse photocurrents from the kinetic contributions.

1. identifying mirror-symmetry-breaking responses

Although the property (i) is extracted from Eqs. (39) and (44), which are valid only for ideal electron gases, intuitively, it should also be held when the relaxation effects are taken into account, provided that the external field is the only agent responsible for mirror-symmetry breaking. This is confirmed in all our numerical tests and demonstrated for the spin polarization components

$S^z(t)$ and $S^\parallel(t)$ in Fig. 5 and for the transverse component of the photocurrent's two contributions, $j_{so}^\perp(t)$ and $j_K^\perp(t)$ in Fig. 6 for both ideal electron gases (upper panels) and the calculations with relaxation included (lower panels). There the signs of brown dashdot lines (for $\varphi_e = 0.25\pi$) are just opposite to that of green dotted lines (for $\varphi_e = \pi - 0.25\pi$). On the contrary, for physical quantities whose non-vanishing values do not arise from mirror-symmetry-breaking effect, namely, $S^\perp(t)$ and $j^\parallel(t)$, the responses obtained under one polarization and that under the mirror-reflected polarization are the same (see Fig. 8 in Ref. [41]). Many choices of φ_e have been tested and give the same conclusion (see Fig. 9 with its discussion in Ref. [41]). Therefore, by comparing the responses induced at a polarization \hat{e} with those induced by the mirror reflection of \hat{e} , one knows if this is a mirror-symmetry-breaking induced response.

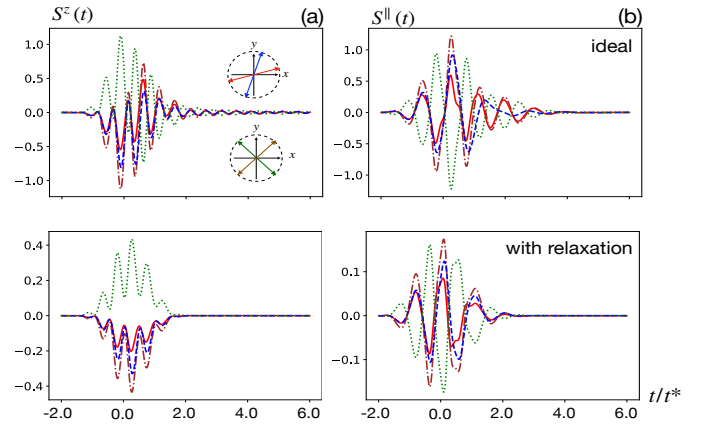


Figure 5: Transient spin polarization components ((a) for out-of-plane and (b) for in-plane), induced by various linearly polarized pulse fields that break the mirror symmetry without (upper panel) and with (lower panel) relaxation effects. The angles of the linear polarizations illustrated here are $\varphi_e = 0.1\pi$ (red solid), $\varphi_e = 0.4\pi$ (blue dashed), $\varphi_e = 0.25\pi$ (brown dash-dot) and $\varphi_e = 0.75\pi$ (green dotted). The lower inset in the upper panel of (a) emphasizes the two polarizations for the brown and the green curves are mirror reflection to each other. In all plots, the signs of these two curves remain opposite to each other in all time. The upper inset in the upper panel of (a) indicates the polarizations for the red and the blue curves deviate respectively from the x -axis and y -axis by the same angle $\delta\varphi = 0.1\pi$. In all plots, these two curves only overlap for a short time before $t = 0$. Their later separation manifests that the two mirror lines associated with different effective masses (anisotropic effects) are inequivalent. The same set of other parameters used in Fig. 4 is used here.

2. distinguishing spin-mediated from charge-mediated processes in photocurrents by anisotropy

While (i) has been found to be true in all our numerical tests for mirror-symmetry-breaking induced quantities,

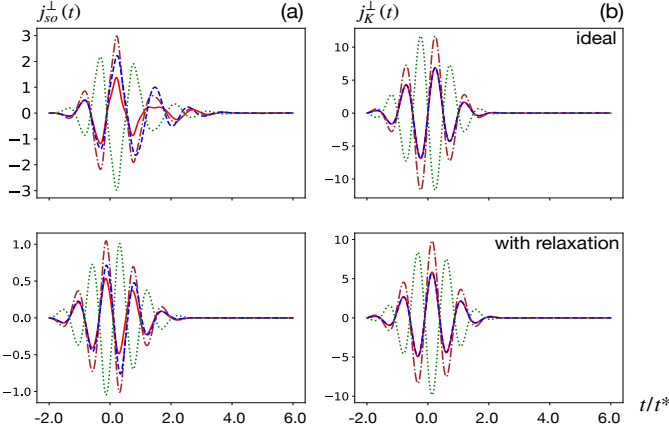


Figure 6: Time evolutions of the transverse components of the spin-mediated (a) and charge-mediated contributions (b) to the photocurrent without (upper panel) and with (lower panel) relaxation effects. The same parameters and color codes used in Fig. 5 are used here.

namely, $S^z(t)$, $S^\parallel(t)$, $j_{so}^\perp(t)$ and $j_K^\perp(t)$, the holding of point (ii) is not even intuitive. To examine this point, we define

$$\Delta_{\delta\varphi} S^\alpha(t) \equiv S^\alpha(t)|_{\varphi_e=\delta\varphi} - S^\alpha(t)|_{\varphi_e=\pi/2-\delta\varphi}, \quad (45)$$

with $0 \leq \delta\varphi \leq \pi/2$ to quantify the anisotropy-induced asymmetry in the α -component of the spin polarization when the mirror symmetry is broken by deviating the linear polarization from either of the mirror line by an angle $\delta\varphi$. Here we have $\alpha = \parallel$, $\alpha = \perp$ or $\alpha = z$. Similar definitions are applied to the different part of the photocurrent, namely, $\Delta_{\delta\varphi} j_K^\alpha(t)$ and $\Delta_{\delta\varphi} j_{so}^\alpha(t)$, as well as the total photocurrent $\Delta_{\delta\varphi} j^\alpha(t)$. When $\delta\varphi = 0$, then we go back to the cases where the mirror-symmetry is preserved, namely, $\Delta_{\delta\varphi=0} S^\alpha(t) = \Delta_0 S^\alpha(t)$ and $\Delta_{\delta\varphi=0} j^\alpha(t) = \Delta_0 j^\alpha(t)$. Given that the effective masses associated with each of the mirror lines are not the same, one generally does not intuitively expect $\Delta_{\delta\varphi} S^\alpha(t) = 0$ or $\Delta_{\delta\varphi} j^\alpha(t) = 0$. This special property (ii) is only asserted by Eq. (39) for the behavior of $j_K^\perp(t)$ obtained under the ideal gas assumption and is not guaranteed to be true if the relaxation effects are taken into account. Note also that Eq. (44) (together with Eqs. (30) and (31)) for the transient spin texture is derived for the time $t = t_1$ implying that $\Delta_{\delta\varphi} S^{\parallel/z}(t = t_1) = 0$. The appearance of $\Delta_{\delta\varphi} S^{\parallel/z}(t) \neq 0$ is anticipated for later time.

Exemplified with $\delta\varphi = 0.1\pi$, we show that for spin-related quantities, namely, the spin polarization $S^z(t)$ and $S^\parallel(t)$ in Fig. 5 and the spin-sensitive part of the photocurrent $j_{so}^\perp(t)$ in Fig. 6(a), the property (ii) is indeed only well obeyed temporarily and violations of (ii) become quite visible for $t \geq 0$ (see the short-time overlapping between the red solid (for $\varphi_e = 0.1\pi$) and blue dashed (for $\varphi_e = 0.4\pi$) lines and their later departure). This is true for both the ideal case and the case with relaxation. In contrast, for the spin-insensitive

part of the mirror-symmetry-breaking induced photocurrent component, $j_K^\perp(t)$, the curve for the time evolution with $\varphi_e = 0.1\pi$ apparently overlaps with that using $\varphi_e = 0.4\pi$ in Fig. 6(b). A closer look at $\Delta_{\delta\varphi} j_K^\perp(t)$ for electron gases with relaxation effects shows that it is not strictly zero $|\Delta_{\delta\varphi} j_K^\perp(t)| \neq 0$ whereas it is strictly zero in the ideal case. However, its magnitude is comparatively small, namely, $|\Delta_{\delta\varphi} j_K^\perp(t)| \ll |j_K^\perp(t)|_{\varphi_e=\delta\varphi}$ and $|\Delta_{\delta\varphi} j_K^\perp(t)| \ll |j_K^\perp(t)|_{\varphi_e=\pi/2-\delta\varphi}$. The difference between $j_K^\perp(t)|_{\varphi_e=\pi/2-\delta\varphi}$ and $j_K^\perp(t)|_{\varphi_e=\delta\varphi}$ is not visible on the scale of $j_K^\perp(t)$ itself. We therefore directly compare $\Delta_{\delta\varphi} j_K^\perp(t)$ with $\Delta_{\delta\varphi} j_{so}^\perp(t)$ in Fig. 7 (a) and we find the spin-sensitive contribution $\Delta_{\delta\varphi} j_{so}^\perp(t)$ dominates in the anisotropy-induced asymmetry for the transverse component of the total photocurrent, $\Delta_{\delta\varphi} j^\perp(t) = \Delta_{\delta\varphi} j_K^\perp(t) + \Delta_{\delta\varphi} j_{so}^\perp(t)$. On the contrary, the anisotropy-induced asymmetry in the longitudinal component of the photocurrent $\Delta_{\delta\varphi} j^\parallel(t)$, whose existence does not need mirror-symmetry breaking, is dominated by the contribution from the kinetic energy, $\Delta_{\delta\varphi} j_K^\parallel(t)$, instead of the spin-sensitive part, $\Delta_{\delta\varphi} j_{so}^\parallel(t)$ (see Fig. 7 (b)). Therefore, via the anisotropy-induced asymmetry, the contrast between the transverse component with $|\Delta_{\delta\varphi} j_K^\perp(t)| \ll |\Delta_{\delta\varphi} j_{so}^\perp(t)|$ (whose existence requires mirror-symmetry breaking) and the longitudinal component with $|\Delta_{\delta\varphi} j_K^\parallel(t)| \gg |\Delta_{\delta\varphi} j_{so}^\parallel(t)|$ (whose existence does not require mirror-symmetry breaking) of the photocurrent differentiates the spin-mediated contribution to the photocurrent from the contribution purely due to the electrons' kinetic energy.

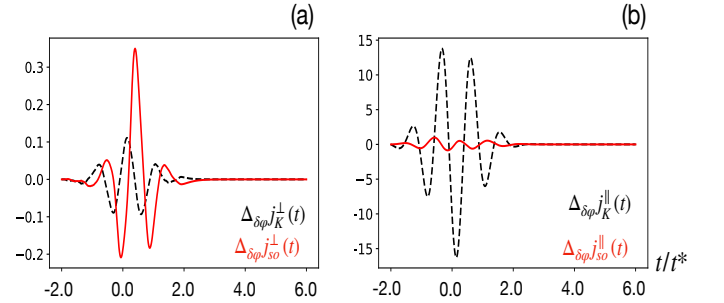


Figure 7: Anisotropy-induced asymmetry with $\delta\varphi = 0.1\pi$ under broken mirror symmetry in the transverse (a) and longitudinal (b) components of the two parts (spin-sensitive and kinetic) of the photocurrent.

Note that previously in Sec. III B with isotropic Rashba SOC where only the longitudinal component of the photocurrent is nonzero, we have observed that the charge-mediated current is larger than the spin-mediated current in amplitude and these two parts of the photocurrent also oscillate with the pulsing electric field in different phases. Similar distinction between the spin-mediated and the charge-mediated contributions has also been observed here for the transverse component of the photocurrent (see Fig. 6). Nevertheless, in the presence of

anisotropic Rashba SOC, the anisotropy-induced asymmetry in the transverse photocurrent yet provides a particular way of distinguishing the spin-mediated from the charge-mediated processes in the photocurrent that is unique to the mirror-symmetry breaking effects.

3. constant polarity in out-of-plane spin polarization

The conclusions obtained in the previous two subsections by examining points (i) (sign reversal upon mirror reflection of polarization) and (ii) (spin-mediated process dominates over charge-mediated ones in the anisotropy-induced asymmetry) have been verified for both ideal electron gases and electron gases including relaxation effects (see other supporting data in Fig. 9 with its discussion in Ref. [41]). These properties are thus intrinsic to the 2D electron gases with the anisotropic Rashba SOC in question. In addition to these intrinsic properties, the field-induced mirror-symmetry breaking under anisotropic Rashba SOC, giving rise to $S^z(t) \neq 0$ and $S^{\parallel}(t) \neq 0$, also shows an intriguing property that is observed only when the relaxation effects coming from extrinsic scattering are included.

In Sec. III B under the isotropic condition, we have seen that including relaxation can cause subtle modulations on the magnitudes and oscillation phases of the spin polarization with respect to their ideal counterparts. Similar phenomena have been observed here with anisotropic Rashba SOC (see Fig. 5). More differently, with the mirror symmetry being broken by the external field, comparing calculations without and with relaxation effects reveals that the sign of $S^z(t)$ remains unchanged during the whole course of its time evolution when relaxation effects are included (lower panel of Fig. 5(a)). The signs of the other spin components (as well as of $S^z(t)$ calculated assuming ideal electron gases) keep alternating over time (other parts of Fig. 5). This property of constant polarity, namely, the sign does not change with time, of $S^z(t)$ has been verified for many other choices of the parameters (see supporting examples in Fig. 10 which includes data of $S^{\perp}(t)$ showing alternating signs).

Note that previous studies of CISP [1, 18, 36] using Rashba SOC with static electric fields show that the CISP is generally realized through the steady non-equilibrium distribution of the electrons' momenta that is determined by both the internal relaxation mechanism and the external field. There, CISP occurs to the in-plane component S^{\perp} whose sign is determined by the fixed direction of the static electric field. Here in the transient regime with electric field pulses, we find that the transient CISP shares similarity with its static counterpart despite obvious differences. On one hand, the time-independence of the sign of the out-of-plane component $S^z(t)$ is due to the internal relaxation mechanism. On the other hand, the sign itself is determined by the fixed linear polarization direction of the applied time-dependent field. Since the transient CISP with time-independent polarity oc-

curs to the out-of-plane component, in contrast to the preference of the in-plane component S^{\perp} in the static case, the involvement of the transient regime indeed offers an alternative route for realizing CISP, taking the advantage of the anisotropy of the Rashba SOC.

IV. CONCLUSION

In summary, we have studied the transient photocurrent and spin polarization responses to laser pulses with various linear polarization orientations in a 2D electron gas with anisotropic Rashba SOC, where the anisotropy arises from the difference in effective masses along orthogonal directions. We aim to understand how the field-induced transient symmetry breaking coordinates with the anisotropic effects of the SOC to play a role on discerning the spin-mediated from the charge-mediated processes in the transient photocurrents and on the consequent transient spin polarization.

To extract the spin-mediated processes from the photocurrent-related signals, a well-established experimental procedure is to analyze these signals by continuously varying the polarization of the exciting lasers crossing both the circular and the linear polarization regimes. This is applicable to both continuous illuminations (exemplified in Ref. [2]) and ultrafast pulses (with examples in [6, 9]). It is also generally applicable to materials whose responses to varied polarizations are anticipated to vary concomitantly. However, it is not always straightforward to relate the results to the specific type of SOC that dominates the spin-mediated responses. Here, from a theoretical point of view, we approach the issue of separating the spin-mediated process from others by starting with a common way of modeling electron gases with SOC effects, which is realized by a Hamiltonian that is a sum of the kinetic energy and the SOC. By separating contributions to the photocurrent into two terms, one from the kinetic energy and the other from the SOC respectively, we have arrived clear definitions that are themselves distinct between spin-mediated (contributed by the SOC term) and charge-mediated (contributed by the kinetic-energy term) processes in the photocurrent (see Eq. (21)). In particular, we want to differentiate spin-mediated from charge-mediated processes from a transient perspective. Although the feasibility of making such separation of contributions to the photocurrent is independent of the particular type of the SOC in question, how the spin-mediated part of the photocurrent differs from the charge-mediated part should at least be specifically rooted to the underlying SOC that gives rise to such distinction.

By specifying the SOC be the anisotropic Rashba type that is linear in momentum, we found that, irrespective whether or not the two effective masses are equal, the transient charge-mediated photocurrent is always larger in amplitude in comparison to the spin-mediated part. These two parts also oscillate with the oscillating elec-

tric field of the exciting pulse with different phases. This suggests a possibility of fitting emitted electromagnetic waves, proportional to $d\mathbf{j}(t)/dt$ [60], in the transient regime by summing two unequal and phase-shifted components to extract respectively contributions from the spin-mediated and charge-mediated processes to ultrafast emissions. However, more restrictions are needed to eliminate ambiguities in choosing the mathematical forms of these fitting terms.

In this respect, the anisotropic characters of the Rashba SOC studied here and the effect of field-induced transient symmetry breaking can play a role on providing restrictions. When the anisotropy of the Rashba SOC is present, the system possesses mirror symmetry in its equilibrium state. Breaking this mirror symmetry by applying a linearly polarized laser pulse can trigger transverse component of the photocurrent to appear. This component is not available if the mirror symmetry is not broken. The sign of this transverse photocurrent can be reversed by performing mirror reflection on the linear polarization of the applied field pulses. This gives one obvious restriction on fitting the real-time current (and its time derivative proportional to emissions) for the transverse components. For the longitudinal component, our calculations show that the mirror reflection of the laser polarization does not alter the current. This also provides a restriction on fitting the longitudinal current. Further hint on possible restrictions on fitting the current can be found through the asymmetry between the photocurrent found at two polarizations that are equal deviations from the two mirror lines. For the transverse component, significant anisotropy-induced asymmetry is found in the spin-mediated contribution to the photocurrent while such asymmetry is relatively small in the charge-mediated part. For the longitudinal component, this trend is reversed. This hints that different restrictions on the fitting terms for the transverse and the longitudinal components of the photocurrent-associated emissions should be applied. The above distinction between spin-mediated part of the photocurrent and the charge-mediated part thus relies on the use of only linearly polarized pulses in manifesting the underlying anisotropy of the Rashba SOC, without involving circular polarization of the exciting fields.

The effects of transient mirror-symmetry breaking are especially intriguing in regards of the consequences on the induced spin polarization. With isotropic Rashba SOC, only the in-plane spin polarization, whose direction is perpendicular to the applied electric field, can

be induced. With anisotropic Rashba SOC, the transient breaking of the mirror symmetry induces not only a nonzero component of the in-plane spin polarization that is parallel to the applied electric field but also very noticeably an out-of-plane spin polarization. While the in-plane components of the spin polarization keep alternating their polarities (signs) in time, the polarity of the out-of-plane spin component is found to be constant over time. For its high relevance to device concepts, special efforts have been spent to generate out-of-plane spin polarization in 2D systems under the name of CISP from a multitude of symmetry-breaking mechanisms that are inherited to the SOC host materials, evoking non-Rashba physics in 2D ferromagnets [37] and the use of planar crystals with lower crystalline symmetries [61]. Here, by going to the transient regime, the rise of the out-of-plane constant-polarity spin polarization is demonstrated with a Rashba Hamiltonian that contains only in-plane spin components whose equilibrium state is fully characterized by a high symmetry C_{2v} group. The symmetry-breaking involved here is not inherited to the SOC hosting system, but purely comes from the external pulse that causes a transient non-equilibrium state with non-vanishing out-of-plane spin polarization.

Due to the limited scope of the present study, where we have only focused on one specific realization of anisotropic SOC in 2D, as detailed in Sec. II, there are still many other questions worth of further investigation in the general direction of ultrafast laser effects in solid-state spintronics with the anisotropy realized by various means briefly reviewed in the introduction. We hope the present study can contribute a bit of progress and further guide us in exploring this important direction.

Acknowledgments

We thank Prof. Feng-Chuan Chuang for raising our attention to the on-going research interests about anisotropic Rashba SOC effects. MWYT also thanks useful discussion with Prof. Ting-Kuo Lee. JPC acknowledges financial support from the Ministry of Science and Technology, Taiwan (Grant No. 109-2112-M-018-008-MY3). CWL thanks the support by National Science and Technology Council of the Republic of China, Taiwan (Grant No.'s 109-2112-M-009-020-MY3, 109-2124-M-009-003-MY3 and 110-2119-M-A49-002-MBK).

[1] P. Hosur, Circular photogalvanic effect on topological insulator surfaces: Berry-curvature-dependent response, *Phys. Rev. B* **83**, 035309 (2011).
 [2] J. McIver, D. Hsieh, H. Steinberg, P. Jarillo-Herrero, and N. Gedik, Control over topological insulator photocurrents with light polarization, *Nat. Nanotechnol.* **7**, 96

(2012).
 [3] A. Junck, G. Refael, and F. von Oppen, Photocurrent response of topological insulator surface states, *Phys. Rev. B* **88**, 075144 (2013).
 [4] J. Duan, N. Tang, X. He, Y. Yan, S. Zhang, X. Qin, X. Wang, X. Yang, F. Xu, Y. Chen, W. Ge, and B. Shen,

- Identification of Helicity-Dependent Photocurrents from Topological Surface States in Bi_2Se_3 Gated by Ionic Liquid, *Sci. Rep.* **4**, 4889 (2014).
- [5] P. Olbrich, L. E. Golub, T. Herrmann, S. N. Danilov, H. Plank, V. V. Bel'kov, G. Mussler, Ch. Weyrich, C. M. Schneider, J. Kampmeier, D. Grützmacher, L. Plucinski, M. Eschbach, and S. D. Ganichev, Room-Temperature High-Frequency Transport of Dirac Fermions in Epitaxially Grown Sb_2Te_3 - and Bi_2Te_3 -Based Topological Insulators, *Phys. Rev. Lett.* **113**, 096601 (2014).
- [6] C. Kastl, C. Karnetzky, H. Karl, and A. W. Holleitner, Ultrafast helicity control of surface currents in topological insulators with near-unity fidelity, *Nat. Commun.* **6**, 6617 (2015).
- [7] K. N. Okada, N. Ogawa, R. Yoshimi, A. Tsukazaki, K. S. Takahashi, M. Kawasaki, and Y. Tokura, Enhanced photogalvanic current in topological insulators via Fermi energy tuning, *Phys. Rev. B* **93**, 081403(R) (2016).
- [8] L. Braun, G. Mussler, A. Hruban, M. Konczykowski, T. Schumann, M. Wolf, Münzenberg, L. Perfetti, and T. Kampfrath, Ultrafast photocurrents at the surface of the three-dimensional topological insulator Bi_2Se_3 , *Nat. Commun.* **7**, 13259 (2016).
- [9] C.-M. Tu, Y.-C. Chen, P. Huang, P.-Y. Chuang, M.-Y. Lin, C.-M. Cheng, J.-Y. Lin, J.-Y. Juang, K.-H. Wu, J.-C. A. Huang, W.-F. Pong, T. Kobayashi, and C.-W. Luo, Helicity-dependent terahertz emission spectroscopy of topological insulator Sb_2Te_3 thin films, *Phys. Rev. B* **96**, 195407 (2017).
- [10] D. Yagodkin, L. Nádorník, O. Gueckstock, C. Gahl, T. Kampfrath and K. I. Bolotin, Ultrafast photocurrents in MoSe_2 probed by terahertz spectroscopy, *2D Mater.* **8**, 025012 (2021).
- [11] R. Raimondi, M. Leadbeater, P. Schwab, E. Caroti, and C. Castellani, Spin-orbit induced anisotropy in the magnetoconductance of two-dimensional metals, *Phys. Rev. B* **64**, 235110 (2001).
- [12] M. Trushin and J. Schliemann, Anisotropic current-induced spin accumulation in the two-dimensional electron gas with spin-orbit coupling, *Phys. Rev. B* **75**, 155323 (2007).
- [13] C. M. Wang, Anisotropic magnetoresistance in a two-dimensional electron system with Rashba and Dresselhaus spin-orbit coupling, *Phys. Rev. B* **82**, 165331 (2010).
- [14] K. W. Kim, K. J. Lee, H. W. Lee, and M. D. Stiles, Perpendicular magnetic anisotropy of two-dimensional Rashba ferromagnets, *Phys. Rev. B* **94**, 184402 (2016).
- [15] A. Johansson, J. Henk, and I. Mertig, Theoretical aspects of the Edelstein effect for anisotropic two-dimensional electron gas and topological insulators, *Phys. Rev. B* **93**, 195440 (2016).
- [16] S. Saberi-Pouya, T. Vazifeshenas, T. Salavati-fard, M. Farmanbar, and F. M. Peeters, Strong anisotropic optical conductivity in two-dimensional puckered structures: The role of the Rashba effect, *Phys. Rev. B* **96**, 075411 (2017).
- [17] K. Wolff, R. Eder, R. Schäfer, R. Schneider, and D. Fuchs, Anisotropic electronic transport and Rashba effect of the two-dimensional electron system in (110) SrTiO_3 -based heterostructures, *Phys. Rev. B* **98**, 125122 (2018).
- [18] L. L. Tao and E. Y. Tsymlal, Spin-orbit dependence of anisotropic current-induced spin polarization, *Phys. Rev. B* **104**, 085438 (2021).
- [19] Z. Feng, H. Qiu, D. Wang, C. Zhang, S. Sun, B. Jin and W. Tan, Spintronic terahertz emitter, *J. Appl. Phys.* **129**, 010901 (2021).
- [20] T. S. Seifert, L. Chen, Z. Wei, T. Kampfrath, J. Qi, Spintronic sources of ultrashort terahertz electromagnetic pulses, *Appl. Phys. Lett.* **120**, 180401 (2022).
- [21] Y. A. Bychkov and E. I. Rashba, Properties of a 2D electron gas with a lifted spectrum degeneracy, *JETP Lett.*, **39**, 78 (1984).
- [22] A. Manchon, H. C. Koo, J. Nitta, S. M. Frolov, and R. A. Duine, New perspectives for Rashba spin-orbit coupling, *Nat. Mater.* **14**, 871 (2015).
- [23] S. Vajna, E. Simon, A. Szilva, K. Palotas, B. Ujfalussy, and L. Szunyogh, Higher-order contributions to the Rashba-Bychkov effect with application to the Bi/Ag(111) surface alloy, *Phys. Rev. B* **85**, 075404 (2012).
- [24] J. Zhou, W.-Y. Shan, and D. Xiao, Spin responses and effective Hamiltonian for the two-dimensional electron gas at the oxide interface $\text{LaAlO}_3/\text{SrTiO}_3$, *Phys. Rev. B* **91**, 241302(R) (2015).
- [25] L. Sun, X. Ma, J. Liu, and M. Zhao, Laser-driven anisotropic and nonlinear Rashba spin splitting in GaAs monolayer, *Phys. Rev. B* **104**, 085140 (2021).
- [26] T. Hu, F. Jia, G. Zhao, J. Wu, A. Stroppa, and W. Ren, Intrinsic and anisotropic Rashba spin splitting in Janus transition-metal dichalcogenide monolayers, *Phys. Rev. B* **97**, 235404 (2018).
- [27] S.-H. Zhang and B.-G. Liu, Anisotropic Rashba effect and charge and spin currents in monolayer BiTeI by controlling symmetry, *Phys. Rev. B* **100**, 165429 (2019).
- [28] P. A. L. Sino, L.-Y. Feng, R. A. B. Villaos, H. N. Cruzado, Z.-Q. Huang, C.-H. Hsu and F.-C. Chuang, Anisotropic Rashba splitting in Pt-based Janus monolayers PtXY ($X, Y = \text{S, Se, or Te}$), *Nanoscale Adv.*, **3**, 6608 (2021).
- [29] L. L. Tao and E. Y. Tsymlal, Perspectives of spintextured ferroelectrics, *J. Phys. D* **54**, 113001 (2021).
- [30] A. Manchon and S. Zhang, Theory of nonequilibrium intrinsic spin torque in a single nanomagnet, *Phys. Rev. B* **78**, 212405 (2008).
- [31] C. Xiao and Q. Niu, Semiclassical theory of spin-orbit torques in disordered multiband electron systems, *Phys. Rev. B* **96**, 045428 (2017).
- [32] F. Freimuth, S. Blügel, and Y. Mokrousov, Charge and spin photocurrents in the Rashba model, *Phys. Rev. B* **103**, 075428 (2021).
- [33] T. Oguchi and T. Shishidou, The surface Rashba effect: a $k \cdot p$ perturbation approach, *J. Phys. Condens. Matter* **21**, 092001 (2009).
- [34] E. Simon, A. Szilva, B. Ujfalussy, B. Lazarovits, G. Zarand, and L. Szunyogh, Anisotropic Rashba splitting of surface states from the admixture of bulk states: Relativistic ab initio calculations and $k \cdot p$ perturbation theory, *Phys. Rev. B* **81**, 235438 (2010).
- [35] Z. S. Popović, J. M. Kurdestany, and S. Satpathy, Electronic structure and anisotropic Rashba spin-orbit coupling in monolayer black phosphorus, *Phys. Rev. B* **92**, 035135 (2015).
- [36] V. M. Edelstein, Spin polarization of conduction electrons induced by electric current in two-dimensional asymmetric electron systems, *Solid State Commun.* **73**, 233 (1990). See also Refs. [18, 37] for recent and more focused accounts on CISP.
- [37] X. Li, H. Chen, and Q. Niu, Out-of-plane carrier spin in transition-metal dichalcogenides under electric current,

- PNAS **117**, 16749 (2020).
- [38] A. G. Aronov, Yu. B. Lyanda-Geller, and G. E. Pikus, Spin polarization of electrons by an electric current, *Sov. Phys. JETP* **73**, 537 (1991).
- [39] G. Vignale and I. V. Tokatly, Theory of the nonlinear Rashba-Edelstein effect: The clean electron gas limit, *Phys. Rev. B* **93**, 035310 (2016).
- [40] N. Sirica, P. P. Orth, M. S. Scheurer, Y. M. Dai, M.-C. Lee, P. Padmanabhan, L. T. Mix, S. W. Teitelbaum, M. Trigo, L. X. Zhao, G. F. Chen, B. Xu, R. Yang, B. Shen, C. Hu, C.-C. Lee, H. Lin, T. A. Cochran, S. A. Trugman, J.-X. Zhu, M. Z. Hasan, N. Ni, X. G. Qiu, A. J. Taylor, D. A. Yarotski and R. P. Prasankumar, Photocurrent-driven transient symmetry breaking in the Weyl semimetal TaAs, *Nat. Mater.* **21**, 62 (2022).
- [41] Supplementary materials containing Sec. A: Fermi surface under anisotropic Rashba SOC, Sec. B: A time-dependent non-adiabatic kinetic theory and Sec. C: Further supporting data.
- [42] N. W. Ashcroft and N. D. Mermin, *Solid State Physics* (Sounders College, Philadelphia, 1976).
- [43] D. Xiao, M.-C. Chang, and Q. Niu, Berry phase effects on electronic properties, *Rev. Mod. Phys.* **82**, 1959 (2010).
- [44] K. Misaki, S. Miyashita, and N. Nagaosa, Diffusive real-time dynamics of a particle with Berry curvature, *Phys. Rev. B* **97**, 075122 (2018).
- [45] E. V. Gorbar, V. A. Miransky, I. A. Shovkovy, and P. O. Sukhachov, Non-Abelian properties of electron wave packets in the Dirac semimetals A₃Bi (A=Na,K,Rb), *Phys. Rev. B* **98**, 045203 (2018).
- [46] T. Higuchi, C. Heide, K. Ullmann, H. B. Weber, and P. Hommelhoff, Light-field-driven currents in graphene, *Nature (London)* **550**, 224 (2017).
- [47] M. W. Y. Tu, C. Li, and W. Yao, Theory of wave-packet transport under narrow gaps and spatial textures: Nonadiabaticity and semiclassicality, *Phys. Rev. B* **102**, 045423 (2020).
- [48] M. W.-Y. Tu, C. Li, H. Yu, and W. Yao, Non-adiabatic Hall effect at Berry curvature hot spot, *2D Mater.* **7**, 045004 (2020).
- [49] C. Li, M. W.-Y. Tu and W. Yao, Revealing the non-adiabatic and non-Abelian multiple-band effects via anisotropic Hall conduction in bilayer graphene, *2D Mater.* **8**, 045012 (2021).
- [50] We denote by t_{off} as the time after which the electric field is forever switched off, namely, $\mathbf{E}(t \geq t_{\text{off}}) = 0$. For $t > t_{\text{off}}$, the first term of Eq. (18a), namely, Eq. (18b), simply gives $\bar{\rho}_{\mathbf{k}}(t) = \rho_{\mathbf{k}t_{\text{off}}}^{\text{eq}}$ since there is no longer field-induced band hybridization effect. For the second term in Eq. (18a), we can separate the domain for the time integral of Eq. (18c) into two intervals, namely, one for $[t_0, t_{\text{off}}]$ and one for $[t_{\text{off}}, t]$. When the integration variable t' lies in $[t_0, t_{\text{off}}]$, the part of the integrand $P(t, t')$ can be decomposed to $P(t, t') = P(t, t_{\text{off}})P(t_{\text{off}}, t')$. One easily observe that $P(t, t_{\text{off}}) \rightarrow 0$ for $t - t_{\text{off}}$ being much greater than the largest among the scattering times $\tau_{\mathbf{k}}$'s and the integral on the interval $[t_0, t_{\text{off}}]$ becomes zero. Since for $t > t_{\text{off}}$, the momentum becomes a constant $\mathbf{k}_t = \mathbf{k}_{t_{\text{off}}}$ and $\bar{\rho}_{\mathbf{k}}(t) = \bar{\rho}_{\mathbf{k}}(t_{\text{off}}) = \rho_{\mathbf{k}t_{\text{off}}}^{\text{eq}}$ commutes with $U_{\mathbf{k}}(t, t') = \exp\{-(i/\hbar)(t-t')\mathcal{H}(\mathbf{k}_{t_{\text{off}}})\}$, then $\bar{\rho}_{\mathbf{k}}^U(t, t') = \rho_{\mathbf{k}t_{\text{off}}}^{\text{eq}}$ becomes independent of t' so $\partial \bar{\rho}_{\mathbf{k}}^U(t, t') / \partial t' = 0$ leading the integral on the interval $[t_{\text{off}}, t]$ to be zero as well. Therefore, for $t - t_{\text{off}} \gg \max_{\mathbf{k}} \tau_{\mathbf{k}}$, Eq. (18c) gives $\delta \rho_{\mathbf{k}}(t) = 0$ finally resulting $\rho_{\mathbf{k}}(t) = \rho_{\mathbf{k}t_{\text{off}}}^{\text{eq}}$. Substituting such density matrix to Eqs. (21) and (24) then yields $\mathbf{j}(t) = 0$ and $\mathbf{S}(t) = 0$ for $t - t_{\text{off}} \gg \max_{\mathbf{k}} \tau_{\mathbf{k}}$.
- [51] J. Sinova, D. Culcer, Q. Niu, N. A. Sinitsyn, T. Jungwirth, and A. H. MacDonald, Universal Intrinsic Spin Hall Effect, *Phys. Rev. Lett.* **92**, 126603 (2004).
- [52] Previous studies of the single wave packet dynamics under adiabatic driving show that a single wave-packet observable at time t gains its time dependence purely through \mathbf{k}_t [3, 4, 48]. This simplifies the texture characterization from $\langle \boldsymbol{\sigma} \rangle(\mathbf{k}, t)$ to simply $\langle \boldsymbol{\sigma} \rangle(\mathbf{k}_t)$. In particular, the Rashba-texture induced intrinsic spin Hall effect is realized through the out-of-plane spin component $\langle \sigma_z \rangle(\mathbf{k}_t)$ [51]. Following the adiabatic evolution of Eq. (15) (details exemplified in Refs. [3, 4, 48])), we find that
- $$\langle \sigma_z \rangle(\mathbf{k}_t) = (-e) \frac{\mathbf{k}_t \times \mathbf{E}}{\alpha_R |\mathcal{X}_K(r_A) \mathbf{k}_t|^3}, \quad (46)$$
- for which $\mathcal{X}_K(r_A)$ is the anisotropic scaling tensor in Eq. (8) of the main text. By setting $r_A = 1$ as the isotropic limit, Eq. (46) reproduces the result in Ref. [51].
- [53] K. S. Denisov, Electric field effect on electron gas spins in two-dimensional magnets with strong spin-orbit coupling, *Phys. Rev. B* **105**, 045413 (2022).
- [54] The Berry curvature of the band $n = \pm$ is defined by $\mathcal{B}_n(\mathbf{k}) = \nabla_{\mathbf{k}} \times \mathcal{R}_{n,n}(\mathbf{k})$. By getting the eigenfunction of Eq. (1), we find $\mathcal{B}_n(\mathbf{k}) = 0$ for all \mathbf{k} 's.
- [55] M. W.-Y. Tu, W.-M. Zhang, J. Jin, O. Entin-Wohlman, and A. Aharony, Transient quantum transport in double-dot Aharonov-Bohm interferometers, *Phys. Rev. B* **86**, 115453 (2012).
- [56] M. W.-Y. Tu, A. Aharony, W.-M. Zhang, and O. Entin-Wohlman, Real-time dynamics of spin-dependent transport through a double-quantum-dot Aharonov-Bohm interferometer with spin-orbit interaction, *Phys. Rev. B* **90**, 165422 (2014).
- [57] Opposite to the present emphasis on how the transient spin texture can reveal the light-induced effects that break the properties (symmetry) of the original electronic system, a recent study has entirely focused on how the information about the properties of the targeted electronic system (the helicity and the mass sign of a Dirac model) can be maintained on the transient spin texture [58]
- [58] X.-X. Zhang and N. Nagaosa, Nonequilibrium topological spin textures in momentum space, *PNAS* **119**, e2116976119 (2022).
- [59] L. Onsager, Reciprocal Relations in Irreversible Processes. I, *Phys. Rev.* **37**, 405 (1931).
- [60] J. Shan and T.F. Heinz in *Ultrafast Dynamical Processes in Semiconductors* vol. 92, 1-56 (Topics in Applied Physics, 2004).
- [61] D. MacNeill, G. M. Stiehl, M. H. Guimaraes, R. A. Buhrman, J. Park, and D. C. Ralph, Control of spin-orbit torques through crystal symmetry in WTe₂/ferromagnet bilayers, *Nat. Phys.* **13**, 300 (2017).

Exploiting anisotropic Rashba effects on real-time photocurrents and spin polarization for transient symmetry breaking

Supplementary Material

Matisse Wei-Yuan Tu,^{1,2,*} Jyh-Pin Chou,³ and Chih-Wei Luo^{4,5,6}

¹*Fritz Haber Center for Molecular Dynamics, Institute of Chemistry, The Hebrew University of Jerusalem, Jerusalem 91904 Israel*

²*Center for Theoretical and Computation Physics, Department of Physics, National Sun Yat-sen University, Kaohsiung 80424, Taiwan*

³*Department of Physics, National Changhua University of Education, Changhua 50007, Taiwan*

⁴*Department of Electrophysics and Institute of Physics, National Yang Ming Chiao Tung University, Hsinchu 30010, Taiwan*

⁵*National Synchrotron Radiation Research Center, Hsinchu 30076, Taiwan*

⁶*Taiwan Consortium of Emergent Crystalline Materials (TCECM), National Science and Technology Council, Taipei 10601, Taiwan*

*Electronic address: kerustemiro@gmail.com

Appendix A: Fermi surface under anisotropic Rashba SOC

In the main text, we focus on the nonequilibrium properties induced by driving laser pulses. In the supporting materials, we supplement the knowledge on the shape of the equilibrium fermi surface under anisotropic Rashba SOC.

The Rashba SOC defines a reciprocal length scale,

$$k_{\text{so}}^* = \frac{m_r \alpha_R}{\hbar^2}, \quad (\text{A1})$$

and an energy scale,

$$\varepsilon_{\text{so}}^* = \frac{m_r \alpha_R^2}{2\hbar^2}. \quad (\text{A2})$$

In the polar coordinate, \mathbf{k} is specified by $\mathbf{k} = (k, \theta)$. At each θ , the lower-energy band $\varepsilon_-(\mathbf{k})$ reaches its minimum when k reaches $k_{\text{so}}(\theta) = [\mathcal{I}_{\text{SO}}(r_A, \theta) / \mathcal{I}_{\text{K}}(r_A, \theta)] k_{\text{so}}^*$ (see Eqs. (4) and (10) for the definitions of $\mathcal{I}_{\text{K}}(r_A, \theta)$ and $\mathcal{I}_{\text{SO}}(r_A, \theta)$ in the main text respectively). The energy for the band edge for a fixed θ is thus given by $\varepsilon_{\text{so}}^{\text{so}}(\theta) \equiv \varepsilon_-(k_{\text{so}}(\theta), \theta)$ as

$$\varepsilon_{\text{so}}^{\text{so}}(\theta) = -\frac{\mathcal{I}_{\text{SO}}^2(r_A, \theta)}{\mathcal{I}_{\text{K}}(r_A, \theta)} \varepsilon_{\text{so}}^* < 0. \quad (\text{A3})$$

We are only interested in the low-energy regime where the equilibrium fermi energy ε_F is nearby the band-edge energy, namely, $\min_{\theta} \varepsilon_{\text{so}}^{\text{so}}(\theta) \lesssim \varepsilon_F < 0$. Note that in $\varepsilon_{\text{so}}^{\text{so}}(\theta)$, the positive dimensionless factor $[\mathcal{I}_{\text{SO}}^2(r_A, \theta) / \mathcal{I}_{\text{K}}(r_A, \theta)]$ is bounded between $\min[\sqrt{r_A}, \sqrt{1/r_A}]$ and $\max[\sqrt{r_A}, \sqrt{1/r_A}]$. It is sufficient to consider only $r_A \geq 1$ without loss of generality. Consequently, since both ε_F and $\varepsilon_{\text{so}}^{\text{so}}(\theta)$ are negative (while the kinetic energy is positive), we work with their absolute values and Eq. (A3) indicates that

$$\frac{1}{\sqrt{r_A}} \varepsilon_{\text{so}}^* \leq |\varepsilon_{\text{so}}^{\text{so}}(\theta)| \leq \sqrt{r_A} \varepsilon_{\text{so}}^*. \quad (\text{A4})$$

In the isotropic limit $r_A = 1$, it is well-known that the shape of the fermi surface is described as an annulus formed in the area between two fermi wave vectors of lengths k_F^+ and k_F^- respectively, in which $k_F^{\pm} = k_{\text{so}}^* \left\{ 1 \pm \sqrt{1 + \varepsilon_F / \varepsilon_{\text{so}}^*} \right\}$. This is a special case of the more general dependence of the lengths of the fermi wave vectors on the angle θ as a manifestation of the SOC anisotropy, namely,

$$k_F^{\pm}(r_A, \theta) = k_{\text{so}}^* \left\{ \frac{\mathcal{I}_{\text{SO}}(r_A, \theta)}{\mathcal{I}_{\text{K}}(r_A, \theta)} \pm \sqrt{\frac{|\varepsilon_{\text{so}}^{\text{so}}(\theta)| - |\varepsilon_F|}{\varepsilon_{\text{so}}^* \mathcal{I}_{\text{K}}(r_A, \theta)}} \right\}, \quad (\text{A5})$$

where $\varepsilon_{\text{so}}^{\text{so}}(\theta)$ is found in Eq. (A3). Clearly $k_F^{\pm}(r_A = 1, \theta) = k_F^{\pm}$ since $\mathcal{I}_{\text{SO}}(r_A = 1, \theta) = \mathcal{I}_{\text{K}}(r_A = 1, \theta) = 1$ and we go back to the isotropic limit.

Increasing r_A further away from the isotropic limit $r_A > 1$ lowers the lower bound of $|\varepsilon_{\text{so}}^{\text{so}}(\theta)|$ as $\varepsilon_{\text{so}}^* / \sqrt{r_A}$ becomes smaller. However as long as $\varepsilon_{\text{so}}^* / \sqrt{r_A} > |\varepsilon_F|$, the fermi surface, though distorted from a perfect annulus, remains connected. Increasing r_A to be more anisotropic such that $\varepsilon_{\text{so}}^* / \sqrt{r_A} < |\varepsilon_F|$, the fermi surface becomes fragmented into two disconnected pieces. The value $r_A = r_A^*(\varepsilon_F) = (\varepsilon_{\text{so}}^* / |\varepsilon_F|)^2$ is the onset of fragmented topology at which the two distinct pieces of the fermi surface are only jointed at $\mathbf{k} = (k = k_{\text{so}}^*, \theta = \pm\pi/2)$. Similar phenomena of having fragmented fermi surfaces have been studied in detail in Ref. [1] regarding static CISP by using two Rashba parameters to describe the anisotropy in SOC, in addition to the effective mass anisotropy in the kinetic energy. The disconnectedness of the fermi surfaces can complicate the electronic responses to external fields. To avoid further complications, we will restrict our discussions of transient photocurrent and spin polarization to $r_A < r_A^*(\varepsilon_F)$.

Appendix B: A time-dependent non-adiabatic kinetic theory

Here we give explicit steps for deducing Eq. (18) of the density matrix $\varrho_{\mathbf{k}}(t)$ in the main text by extending the kinetic theory framed in Refs. [2, 3] in Sec. B 1. We start by describing the formulation in the kinetic theory for electron gases, that is common to the circumstances (a),(b) and (c) to be specified in the following. (a): The band gaps and the external electric fields are set to satisfy the adiabatic condition. (b): The band gaps and the external electric fields are not set to satisfy the adiabatic condition but the external electric fields are assumed to be static at times of interests for steady states. (c) The external electric fields are time-dependent and we are interested in the transient regime. We then in Sec. B 1 a briefly review the specification to situations (a) (well established in Refs. [2, 3]) and (b) (detailed in Ref. [4]). After this, how the specification to (c) can be done then becomes obvious in Sec. B 1 b. Since the main focus of the present research is on the time-dependent phenomena, in Sec. B 2, we show that under periodic driving with small amplitudes such that the adiabatic condition is valid, the second-order response calculated using the density matrix given by Eq. (18)) reproduces the well-established quantum nonlinear Hall effect of Ref. [5].

1. A kinetic theory for electron gases as ensemble of wave packets

Let t_0 denotes the time before which the electron gas has remained at equilibrium and the external field is only switched on after t_0 . Let us consider a wave packet whose momentum at time t_0 is $\mathbf{k}_{t_0} = \mathbf{k}$ and it is in an initially occupied band denoted by $|\chi_{t_0}\rangle = |\chi\rangle$. We use the notation (\mathbf{k}, χ) to denote such state. If we assume that there is no scattering, then a wave packet starting at time $t' \geq t_0$ with momentum $\mathbf{k}_{t'}$ in some superposition $|\chi_{t'}\rangle$ of the bands $|u_n(\mathbf{k}_{t'})\rangle$'s will reach at time $t > t'$ a new state with momentum \mathbf{k}_t and a superposition of bands described by $|\chi_t\rangle = U_{\mathbf{k}}(t, t')|\chi_{t'}\rangle$ (see the definition of the evolution operator in Eq. (16) in the main text). The occupation on the state (\mathbf{k}_t, χ_t) is expressed by the density matrix as $\langle \chi_t | \varrho_{\mathbf{k}}(t) | \chi_t \rangle$. The above-described field-driven process is one source of contribution to the occupation $\langle \chi_t | \varrho_{\mathbf{k}}(t) | \chi_t \rangle$.

We now consider how scattering events affect the probability that the occupation $\langle \chi_t | \varrho_{\mathbf{k}}(t) | \chi_t \rangle$ is actually contributed by a wave packet that has coherently driven to the state (\mathbf{k}_t, χ_t) . The effects of scatterings are taken into account by the relaxation-time approximation which consists of two assumptions (i) and (ii) that we will individually introduce in appropriate places. The assumption (i) is that the scattering rate is independent of the form of the electron distribution function. Utilizing (i), we then denote by $1/\tau_{\mathbf{k}}$, the scattering rate for a wave packet carrying momentum \mathbf{k} . By a general argument, one then

finds that the probability for the wave packet to evolve in a scattering-free manner during the time interval $[t', t]$ is given by [2],

$$P(t, t') = \exp \left[- \int_{t'}^t dt'' \tau_{\mathbf{k}_{t''}}^{-1} \right]. \quad (\text{B1})$$

Henceforth, the contribution to $\langle \chi_t | \varrho_{\mathbf{k}}(t) | \chi_t \rangle$ by the above field-driven process is given by

$$g_{\chi_t}^{\text{drift}}(\mathbf{k}_t, t) = \int_{t'=t_0}^{t'=t} dg_{\chi_{t'}}(\mathbf{k}_{t'}, t') P(t, t'), \quad (\text{B2})$$

where $dg_{\chi_{t'}}(\mathbf{k}_{t'}, t')$ is the amount occupation gained into the state $(\mathbf{k}_{t'}, \chi_{t'})$ in an infinitesimal time interval of length dt' around time t' . Note that at $t = t_0$, $g_{\chi}^{\text{drift}}(\mathbf{k}, t_0) = 0$ by the definition of Eq. (B2). So if the initial equilibrium readily has a nonzero occupation on (\mathbf{k}, χ) , this source of contribution to the occupation is not accounted for by Eq. (B2). By including also this contribution, we obtain

$$\langle \chi_t | \varrho_{\mathbf{k}}(t) | \chi_t \rangle = g_{\chi_t}^{\text{drift}}(\mathbf{k}_t, t) + \langle \chi | \varrho_{\mathbf{k}}^{\text{eq}} | \chi \rangle P(t, t_0) \quad (\text{B3})$$

where the appearance of the factor $P(t, t_0)$ in the second term in Eq. (B3) accounts for the fraction of the initial equilibrium occupation that has survived the scattering.

The result Eq. (B3) aided by Eqs. (B1) and (B2) is common to all situations (a),(b) and (c). If we are only interested in the steady states, we then send t_0 to $-\infty$ and $P(t, t_0 = -\infty) = 0$. The occupation on (\mathbf{k}_t, χ_t) simply becomes

$$\langle \chi_t | \varrho_{\mathbf{k}}(t) | \chi_t \rangle = g_{\chi_t}^{\text{drift}}(\mathbf{k}_t, t). \quad (\text{B4})$$

This is the starting point for the construction of the electron distribution function in the kinetic theory framework in Ref. [2] which is the basis also of Refs. [3, 4] for exploring Berry curvature effects under adiabatic and non-adiabatic conditions in the steady-state limits as the circumstances (a) and (b) mentioned above.

To make further progresses from Eq. (B4) (which amounts to further specifying the contents of Eq. (B2)), we need the assumption (ii) of the relaxation-time approximation. This assumption is based on the observation that in the absence of external fields, the collection of scattering events maintains the electronic system to obey some form of the distribution function, e.g., the Fermi-Dirac distribution function that describes the thermal equilibrium of the electron gases. Therefore, with the external field \mathbf{E} being turned on, we assume that there exists some form of distribution function $g_{\chi_{t'}}^0(\mathbf{k}_{t'})$ such that whenever the electron occupation at a momentum $\mathbf{k}_{t'}$ arrives this form, the occupation number should not be changed by the effects of scatterings. In other words, during the infinitesimal interval of length dt' around time t' , the amount of electrons gained into the state $(\mathbf{k}_{t'}, \chi_{t'})$, denoted by $dg_{\chi_{t'}}(\mathbf{k}_{t'}, t')$, should equal to the amount of

electrons lost from the occupation specified by $g_{\chi_{t'}}^0(\mathbf{k}_{t'})$ due to scatterings, namely,

$$dg_{\chi_{t'}}(\mathbf{k}_{t'}, t') = \frac{dt'}{\tau_{\mathbf{k}_{t'}}} g_{\chi_{t'}}^0(\mathbf{k}_{t'}). \quad (\text{B5})$$

Further explicating $g_{\chi_{t'}}^0(\mathbf{k}_{t'})$ then requires the differentiation between the circumstance (a) (under the adiabatic condition) and (b),(c) (not under the adiabatic condition).

a. Steady-state electron distribution function

We now briefly review how Eq. (B5) is further specified to obtain steady-state occupations through performing the time integral in Eq. (B2) with $t_0 \rightarrow -\infty$. If the circumstance (a) is fulfilled, then an electron wave packet starting from one band n at time t' (carrying momentum $\mathbf{k}_{t'}$) still remains at the same band n under a different momentum \mathbf{k}_t at a later time $t > t'$. It is thus sufficient to consider $|\chi_{t'}\rangle = |u_n(\mathbf{k}_{t'})\rangle$ for which we apply the notations, $f_n^0(\mathbf{k}_{t'}) = g_{\chi_{t'}}^0(\mathbf{k}_{t'})$ and $f_n(\mathbf{k}_{t'}, t') = \langle \chi_{t'} | \varrho_{\mathbf{k}}(t') | \chi_{t'} \rangle_{|\chi_{t'}\rangle = |u_n(\mathbf{k}_{t'})\rangle}$ to follow the notational convention in the literatures. In this way, Eq. (B5) is rewritten into

$$df_n(\mathbf{k}_{t'}, t') = \frac{dt'}{\tau_{\mathbf{k}_{t'}}} f_n^0(\mathbf{k}_{t'}), \quad (\text{B6})$$

in which $f_n^0(\mathbf{k}_{t'}) = f^0(\varepsilon_n(\mathbf{k}_{t'}))$ is the Fermi-Dirac distribution function, describing the statistical mixture of the original bands $|u_n(\mathbf{k}_{t'})\rangle$'s. By substituting Eq. (B6) into the right-hand side of Eq. (B2) (with $t_0 \rightarrow -\infty$), the non-equilibrium electron distribution in the steady state, namely, Eq. (B4), can be found by using the integration-by-part technique for the temporal integral. Together with the short-relaxation-time approximation [6], namely,

$$P(t, t') f(t') \approx e^{-\frac{t-t'}{\tau_{\mathbf{k}_t}}} f(t) \quad (\text{B7})$$

for arbitrary function $f(t')$, to simplify the integrand for the integration dt' , the result is $f_n(\mathbf{k}_t, t) = f_n^0(\mathbf{k}_t) + \delta f_n(\mathbf{k}_t)$ where $\delta f_n(\mathbf{k}_t) = -\tau_{\mathbf{k}_t} [\partial f_n^0(\mathbf{k}_t) / \partial \mathbf{k}_t] \cdot \dot{\mathbf{k}}_t$ and $\dot{\mathbf{k}}_t = (-e/\hbar) \mathbf{E}$. This is the well-established steady-state solution ($\partial f_n / \partial t = 0$) to the Boltzmann equation under the relaxation time approximation.

If the adiabatic condition (a) is not fulfilled, then the external electric field can hybridize the bands as we come to the circumstance (b). The hybridized bands, $|u_i(\mathbf{k}_{t'})\rangle$'s, each as a superposition of the original bands $|u_n(\mathbf{k}_{t'})\rangle$'s, depend non-perturbatively on \mathbf{E} and are eigenfunctions of the moving-frame Hamiltonian $\bar{\mathcal{H}}(\mathbf{k}_{t'}, \mathbf{E})$ (see its definition in the texts below Eq. (18) in the main text) with eigenenergies $\mathcal{E}_i(\mathbf{k}_{t'})$'s. The joint action of the decoherence and the electric field \mathbf{E} results

in a statistical mixture of the hybridized bands, leading to

$$g_{\chi_{t'}}^0(\mathbf{k}_{t'}) = \sum_i |\langle u_i(\mathbf{k}_{t'}) | \chi_{t'} \rangle|^2 g_i^0(\mathbf{k}_{t'}), \quad (\text{B8})$$

where $g_i^0(\mathbf{k}_{t'}) = f^0(\mathcal{E}_i(\mathbf{k}_{t'}))$. This casts Eq. (B5) to

$$dg_{\chi_{t'}}(\mathbf{k}_{t'}, t') = \frac{dt'}{\tau_{\mathbf{k}_{t'}}} \sum_i |\langle u_i(\mathbf{k}_{t'}) | \chi_{t'} \rangle|^2 g_i^0(\mathbf{k}_{t'}). \quad (\text{B9})$$

By applying similar procedures that get the steady-state distribution $f_n(\mathbf{k}_t, t)$ from Eq. (B6), here Eq. (B9) finally gives

$$g_i(\mathbf{k}_t, t) = g_i^0(\mathbf{k}_t) + \delta g_i(\mathbf{k}_t), \quad (\text{B10})$$

where

$$\delta g_i(\mathbf{k}_t) = -\tau_{\mathbf{k}_t} \frac{\partial g_i^0(\mathbf{k}_t)}{\partial \mathbf{k}_t} \cdot \left(\frac{-e}{\hbar} \right) \mathbf{E}, \quad (\text{B11})$$

and we have notated $g_i(\mathbf{k}_t, t) = \langle u_i(\mathbf{k}_t) | \varrho_{\mathbf{k}}(t) | u_i(\mathbf{k}_t) \rangle$. How the result of Eq. (B10) reduces to the well-known result of (a) mentioned below Eq. (B6) in the limit of weak electric field has been detailed in Ref. [4]. Together with Eq. (20) (in the main text) for computing the currents, the main results of revealing the Berry curvature effects through the currents in Ref. [3] are also reproduced in Ref. [4] by taking the adiabatic limit.

b. time-dependent electric fields

We are now facilitated to generalize the above construction to the circumstance (c) with time-dependent electric field to obtain $\varrho_{\mathbf{k}}(t)$ for t not far away from t_0 . Since the circumstance (b) is a special case of (c) by taking $t_0 \rightarrow -\infty$ and the electric field to be constant in time, we simply need to restore $\mathbf{E} \rightarrow \mathbf{E}(t')$ in $\bar{\mathcal{H}}(\mathbf{k}_{t'}, \mathbf{E}(t'))$ for specifying $|u_i(\mathbf{k}_{t'})\rangle$ and $\mathcal{E}_i(\mathbf{k}_{t'})$ used in Eq. (B9) (which is substituted to the right-hand side of Eq. (B2)) and apply Eq. (B3) instead of Eq. (B4) to compute $\varrho_{\mathbf{k}}(t)$.

By the use of $P(t, t') / \tau_{\mathbf{k}_{t'}} = \partial P(t, t') / \partial t'$ (see Eq. (B1)), Eq. (B2) becomes

$$g_{\chi_{t'}}^{\text{drift}}(\mathbf{k}_t, t) = \int_{t_0}^t dt' \langle \chi_{t'} | \bar{\varrho}_{\mathbf{k}}(t') | \chi_{t'} \rangle \frac{\partial P(t, t')}{\partial t'}, \quad (\text{B12})$$

where $\bar{\varrho}_{\mathbf{k}}(t') = \sum_i g_i^0(\mathbf{k}_{t'}) |u_i(\mathbf{k}_{t'})\rangle \langle u_i(\mathbf{k}_{t'})|$ (see also Eq. (18b) in the main text). Performing the integral of Eq. (B12) using the integration-by-part method and applying $|\chi_{t'}\rangle = U_{\mathbf{k}}(t', t) |\chi_t\rangle$ for $t_0 \leq t' \leq t$ to turn the right-hand side of Eq. (B3) to the form of $\langle \chi_t | \bullet | \chi_t \rangle$ so that the density matrix $\varrho_{\mathbf{k}}(t)$ can be identified with \bullet in Eq. (B3), the result then is just Eq. (18) of the main text. To recover Eq. (B10) from Eq. (18), in addition to send t_0 to $-\infty$, we also need to apply Eq. (B7).

2. stationary second-order response

We now turn to the verification of Eq. (18) by considering the current (using Eq. (20)) to the second order in the electric field under time-periodic drivings at time t that is far away from t_0 under the adiabatic condition. In this limit, it is widely recognized that the second-order current carries the information of the Berry curvature dipole that serves as the basis of quantum nonlinear Hall effect [5].

Under the adiabatic condition (with gaps being large in comparison to the electric field), the weak applied field only weakly hybridizes the bands. The index i for labeling a hybridized band can thus be reduced to the label of original band n , namely, $|u_n(\mathbf{k}_t)\rangle \approx e^{i\gamma_n(\mathbf{k}_t)} |u_n(\mathbf{k}_t)\rangle + |\delta u_n(\mathbf{k}_t)\rangle$, where $|\delta u_n(\mathbf{k}_t)\rangle$ is the perturbation to the first order in the electric field while to the same order $\mathcal{E}_n(\mathbf{k}_t) \approx \varepsilon_n(\mathbf{k}_t)$ so $g_i^0(\mathbf{k}_t) \approx f_n^0(\mathbf{k}_t)$ (see details in Ref. [4]). This leads to the matrix elements of the velocity operator (see its definition in Eq. (19) of the main text) given by,

$$\langle u_n(\mathbf{k}_t) | \mathbf{V}(\mathbf{k}_t) | u_n(\mathbf{k}_t) \rangle = \mathbf{v}_n^b(\mathbf{k}_t) + \mathbf{v}_n^a(\mathbf{k}_t), \quad (\text{B13})$$

where $\mathbf{v}_n^b(\mathbf{k}_t) = \hbar^{-1} \partial \varepsilon_n(\mathbf{k}_t) / \partial \mathbf{k}_t$ is the normal band velocity and

$$\mathbf{v}_n^a(\mathbf{k}_t) = \left(\frac{-e}{\hbar} \right) \mathcal{B}_n(\mathbf{k}_t) \times \mathbf{E}(t) \quad (\text{B14})$$

is known as the anomalous velocity [3] with $\mathcal{B}_n(\mathbf{k}_t)$ the Berry curvature of the band n (see its definition in the footnote [54] of the main text). Substituting Eq. (18) to Eq. (20) generally gives $\mathbf{j}(t) = \bar{\mathbf{j}}(t) + \delta \mathbf{j}(t)$ for the current, where $\bar{\mathbf{j}}(t) = -e \int d^D \mathbf{k} \text{Tr}(\mathbf{V}(\mathbf{k}_t) \bar{\varrho}_{\mathbf{k}}(t))$ and $\delta \mathbf{j}(t) = -e \int d^D \mathbf{k} \text{Tr}(\mathbf{V}(\mathbf{k}_t) \delta \varrho_{\mathbf{k}}(t))$ where D is the spatial dimension of the system. By the adiabatic approximation (weakly hybridized bands) applied to $\bar{\varrho}_{\mathbf{k}}(t)$ with Eq. (B13), we find that $\bar{\mathbf{j}}(t)$ is only to the first order of $\mathbf{E}(t)$ which gives the usual linear-response Hall current well reviewed in Ref. [3]. The second-order response then must be contained in $\delta \mathbf{j}(t)$.

With the adiabatic condition imposed to the coherent evolution process, namely, $|u_n(\mathbf{k}_t)\rangle = U_{\mathbf{k}}(t, t') |u_n(\mathbf{k}_{t'})\rangle$, rendering $\bar{\varrho}_{\mathbf{k}}^U(t, t') = \sum_n |u_n(\mathbf{k}_t)\rangle \langle u_n(\mathbf{k}_t) | f_n^0(\mathbf{k}_{t'})$ (see the definition of $\bar{\varrho}_{\mathbf{k}}^U(t, t')$ in Eq. (18d) of the main text), the second term of Eq. (18) becomes

$$\delta \varrho_{\mathbf{k}}(t) = - \sum_n |u_n(\mathbf{k}_t)\rangle \langle u_n(\mathbf{k}_t) | \delta f_{n\mathbf{k}}^{(1)}(t) \quad (\text{B15})$$

where

$$\delta f_{n\mathbf{k}}^{(1)}(t) = \int_{t_0}^t dt' P(t, t') \frac{\partial f_n^0(\mathbf{k}_{t'})}{\partial \mathbf{k}_{t'}} \cdot \left(\frac{-e}{\hbar} \right) \mathbf{E}(t'), \quad (\text{B16})$$

in which the term $(\partial f_n^0(\mathbf{k}_{t'}) / \partial \mathbf{k}_{t'}) \cdot (-e/\hbar) \mathbf{E}(t')$ comes from $d f_n^0(\mathbf{k}_{t'}) / dt'$. One therefore has $\delta \mathbf{j}(t) = \delta \mathbf{j}^{(1)}(t) +$

$\delta \mathbf{j}^{(2)}(t)$ where $\delta \mathbf{j}^{(1)}(t) = -e \sum_n \int d^D \mathbf{k} \mathbf{v}_n^b(\mathbf{k}_t) \delta f_{n\mathbf{k}}^{(1)}(t)$ is to the first order in the electric field and $\delta \mathbf{j}^{(2)}(t) = -e \sum_n \int d^D \mathbf{k} \mathbf{v}_n^a(\mathbf{k}_t) \delta f_{n\mathbf{k}}^{(1)}(t)$ accounts for the second-order response.

We now further assume that $\tau_{\mathbf{k}'} = \tau$ (single-relaxation time) for all possible \mathbf{k}' . We also assume that τ is short so that Eq. (B7) can be applied. Nevertheless, we only apply the approximation of Eq. (B7) to just the part $P(t, t')$ ($\partial f_n^0(\mathbf{k}_{t'}) / \partial \mathbf{k}_{t'}$) of the integrand in the integral of Eq. (B16), while the part of the integrand given by $\mathbf{E}(t')$ is left intact [7]. We now impose the time-periodic driving $\mathbf{E}(t') = \text{Re} \left\{ \tilde{\mathbf{E}} e^{i\omega t'} \right\}$ where $\tilde{\mathbf{E}}$ is the time-independent complex electric-field amplitude and take the limit $t_0 \rightarrow -\infty$, we then end up with

$$\delta \mathbf{j}^{(2)}(t) = - \sum_{n\alpha} \int d^D \mathbf{k} f_n^0(\mathbf{k}) \frac{\partial \mathcal{B}_n(\mathbf{k})}{\partial k_\alpha} \times \text{Re} \left\{ \frac{\tau e^3}{2\hbar^2 (1 + i\omega\tau)} \left(\tilde{E}_\alpha \tilde{\mathbf{E}}^* + e^{2i\omega t} \tilde{E}_\alpha \tilde{\mathbf{E}} \right) \right\}, \quad (\text{B17})$$

where the index α runs over the spatial components and in the intermediate procedure, we have identified $d^D \mathbf{k}$ with $d^D \mathbf{k}_t$ and afterwards rewritten \mathbf{k}_t to \mathbf{k} for the integral. The Berry curvature dipole is given by the components of $\partial \mathcal{B}_n(\mathbf{k}) / \partial k_\alpha$. By focusing on one active band n , Eq. (B17) then reproduces the second-order response describing the quantum nonlinear Hall effect in accordance with Ref. [5].

Appendix C: Further supporting data

Fig. 8 is for components of spin polarization and photocurrents, whose existence do not require mirror-symmetry breaking. Here the brown dashed and the green dotted lines, each generated under a linear polarization that is the mirror reflection of the other (illustrated by the lower inset of the plot for $j_K^{\parallel}(t)$ on the left column of Fig. 8), are shown to be overlapping in all plots. This is in contrast to mirror-symmetry breaking induced components (discussed in the main text around its Figs. 5 and 6) where these two lines are opposite in sign. By varying the linear polarization from $\varphi_e = 0.1\pi$ (red solid) to $\varphi_e = 0.4\pi$ (blue dashed) through $\varphi_e = 0.25\pi$ (brown dash-dot), the red solid time-evolution curve gradually resembles that of the blue dash line through the brown dash-dot curve as an intermediate in all plots of Fig. 8. Very differently, for mirror-symmetry breaking induced components plotted in Figs. 5 and 6 of the main text, the red and the blue dashed curves appear to be overlapping for a time about $2\tau_P$ away from t_0 . The transient behaviors of the spin polarization and photocurrent components that require mirror-symmetry breaking and those that do not rely on such symmetry-breaking effect are certainly distinct.

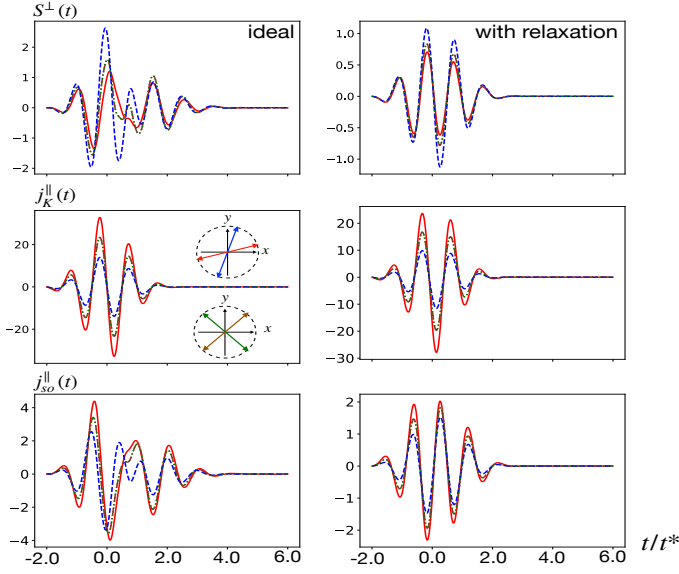


Figure 8: Time-dependence of spin polarization component $S^\perp(t)$ (upper panel) and longitudinal component of the photocurrent, consisting of $j_K^\parallel(t)$ (middle panel) and $j_{so}^\parallel(t)$ (lower panel) that are not induced by mirror-symmetry breaking. Here we use the same parameters and color codes of Fig. 5 of the main text.

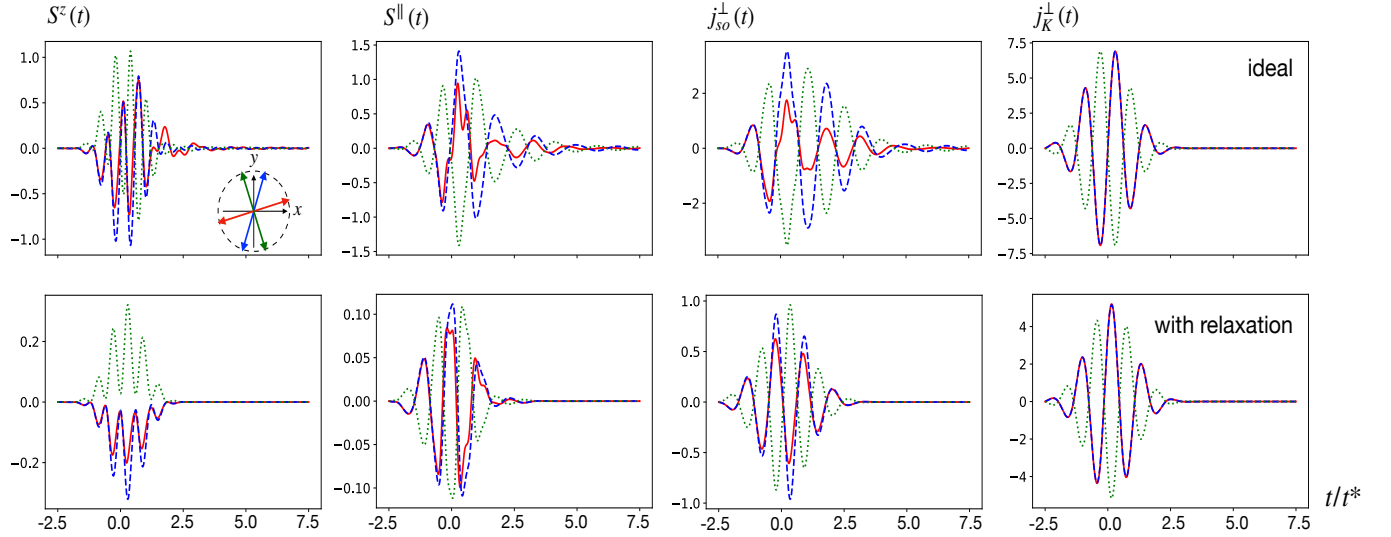


Figure 9: Time evolution of mirror-symmetry-breaking induced spin polarization ($S^z(t)$ and $S^\parallel(t)$) and photocurrent ($j_{so}^\perp(t)$ and $j_K^\perp(t)$) components without (upper panel) and with (lower panel) relaxation effects included ($\tau = 0.2t^*$), calculated with a different set of parameters used in Fig. 5 and Fig. 6 of the main text to demonstrate the same salient effects of transient mirror-symmetry breaking pointed out in the main text. The blue dashed, green dotted and red solid lines are with $\varphi_e = 0.4\pi$, $\varphi_e = 0.6\pi$ and $\varphi_e = 0.1\pi$. The parameters used here are $m_y/m_x = 2.6$, $\varepsilon_F = -0.4\varepsilon_{so}^*$, $E_0 = 0.9E_0^*$ and $\tau_P = 1.25$ with $\omega = (2\pi/t^*)0.8$.

Fig. 9 is for components of spin polarization and photocurrents, whose existence do require mirror-symmetry breaking. The calculations here are run with parameters that are different from those used in Fig. 5 and Fig. 6 of the main text (see captions for detail). Here the blue dashed and green dotted lines are with pulse polarizations characterized by $\varphi_e = 0.4\pi$ and $\varphi_e = 0.6\pi$ (see the inset for the plot of $S^z(t)$ on the upper panel) that are mutually mirror reflection. The signs of these two curves are opposite to each other in all plots (consistent with the findings in the main text). The red solid lines are under $\varphi_e = 0.1\pi$, deviating from the x -axis by the same amount $\delta\varphi = 0.1\pi$ as the polarization for the blue dashed curves deviates from the y -axis (see the same inset for indicating polarization of exciting pulses). For spin-related quantities (the first three columns counted from the left in Fig. 9), these two curves are overlapping temporarily, then the two curves obviously depart from each other around $t \gtrsim 0$. Meanwhile, for the spin-insensitive part of the photocurrent, $j_K^\perp(t)$, these two curves appear to be overlapping with each other all the time. The same characters concluded from the main text about mirror-symmetry induced responses are also found here.

In Fig. 10, the transient dynamics of the three spin po-

larization components, including both in-plane $S^{\perp/\parallel}(t)$

and out-of-plane $S^z(t)$, are plotted under two sets of different physical parameters (one for upper panel and one for the lower panel, see details in the caption). In addition to supporting the constant polarity of the out-of-plane spin polarization as a common result of including relaxation effects in the calculation (the sign of the red solid lines on the right column of Fig. 10 does not change with time), Fig. 10 showing altogether the results from two unrelated sets of parameters also manifests another role of the relaxation effects. It shows that only when extrinsic scattering effects are excluded (the left column), the detailed transient profiles of the spin polarization components are highly sensitive to the parameters characterizing the intrinsic nature of the electron gas (see the apparent difference between the upper and the lower plots in the left column of Fig. 10). However, such visible difference between the spin dynamics from these two sets of parameters defining quantitatively different intrinsic properties of the electron gas becomes less obvious when extrinsic relaxation effects are taken into account (see the similarity between the two plots in the right column of Fig. 10). Furthermore, in the absence of relaxation effects, the three components span in almost the same range of magnitudes (the left panel). On the contrary, when relaxation effects are included, the maximum magnitude $S^\perp(t)$ can achieve is apparently larger than the other two components $S^\parallel(t)$ and $S^z(t)$ (the right panel, see the much larger range of green dotted lines in com-

parison to that of the red solid and blue dashed curves). Such phenomena showing the dominance of $S^\perp(t)$ is also observed for the set of parameters used in Fig. 8 (comparing $S^\perp(t)$ in Fig. 8 with $S^\parallel(t)$ and $S^z(t)$ in Fig. 5 of the main text). The prominence of $S^\perp(t)$ found in the transient regime is consistent with its steady-state counterpart within the general scenario of CISP. For the latter, only the component S^\perp is nonzero due to the symmetry of our starting Hamiltonian (see discussions in the main text).

Collecting the values of Rashba SOC related parameters based on ab initio studies of various materials [8] (Au(110) surface), [9–11] (2D Janus materials), [12](monolayer BiTeI), [13] (monolayer black phosphorus), we find the Rashba energy ε_{so}^* mostly lies in the range from one to tens of meV. For monolayer black phosphorus, the Rashba energy is on the order of a few to tens of μeV . For 110-gold surface, 2D Janus materials, monolayer BiTeI, the Rashba energy converts to a time scale of hundreds femtoseconds to a few picoseconds. For monolayer black phosphorus, it becomes hundred picoseconds to a few nanoseconds. These time scales set the temporal width of the pulse with the central photon energy tuned to accommodate one cycle of oscillation to induce the primary phenomena discussed in this article. Since laser pulses of even shorter duration are experimentally realizable, the above proposed laser pulses should be feasible.

-
- [1] A. Johansson, J. Henk, and I. Mertig, Theoretical aspects of the Edelstein effect for anisotropic two-dimensional electron gas and topological insulators, *Phys. Rev. B* **93**, 195440 (2016).
- [2] N. W. Ashcroft and N. D. Mermin, *Solid State Physics* (Sounders College, Philadelphia, 1976).
- [3] D. Xiao, M.-C. Chang, and Q. Niu, Berry phase effects on electronic properties, *Rev. Mod. Phys.* **82**, 1959 (2010).
- [4] M. W. Y. Tu, C. Li, and W. Yao, Theory of wavepacket transport under narrow gaps and spatial textures: Nonadiabaticity and semiclassicality, *Phys. Rev. B* **102**, 045423 (2020).
- [5] I. Sodemann and L. Fu, Quantum nonlinear Hall effect induced by Berry curvature dipole in time-reversal invariant materials *Phys. Rev. Lett.* **115**, 216806 (2015).
- [6] By assuming the smallness of τ_{k_t} , the value of $P(t, t') f(t')$ becomes non-negligible only for t' near t such that τ_{k_t} is approximated by τ_{k_t} .
- [7] Conventionally, the second-order current is found by solving the Boltzmann equation for one band n , namely, $\partial f_n(\mathbf{k}_t, t) / \partial t + (-e/\hbar) \mathbf{E}(t) \cdot (\partial f_n(\mathbf{k}_t, t) / \partial \mathbf{k}) = -(f_n(\mathbf{k}_t, t) - f_n^0(\mathbf{k}_t)) / \tau$ with $f_n(\mathbf{k}_t, t)$ considered up to the second order in the electric field and one computes the current by $\mathbf{j}(t) = -e \int d^D \mathbf{k} f_n(\mathbf{k}_t, t) \mathbf{v}_n(\mathbf{k}_t)$ where $\mathbf{v}_n(\mathbf{k}_t)$ is given by the right-hand side of Eq. (B13). The partial application of the short-relaxation time approximation Eq. (B7) that leaves the form of $\mathbf{E}(t')$ intact in the relevant time integral should also be employed to solve the Boltzmann equation to yield the result of Eq. (B17).
- [8] E. Simon, A. Szilva, B. Ujfalussy, B. Lazarovits, G. Zarand, and L. Szunyogh, Anisotropic Rashba splitting of surface states from the admixture of bulk states: Relativistic ab initio calculations and $k \cdot p$ perturbation theory, *Phys. Rev. B* **81**, 235438 (2010).
- [9] T. Hu, F. Jia, G. Zhao, J. Wu, A. Stroppa, and W. Ren, Intrinsic and anisotropic Rashba spin splitting in Janus transition-metal dichalcogenide monolayers, *Phys. Rev. B* **97**, 235404 (2018).
- [10] J. Chen, K. Wu, H. Ma, W. Hu, and J. Yang, Tunable Rashba spin splitting in Janus transition metal dichalcogenide monolayers via charge doping, *RSC Adv.* **10**, 6388 (2020).
- [11] P. A. L. Sino, L.-Y. Feng, R. A. B. Villaos, H. N. Cruzado, Z.-Q. Huang, C.-H. Hsu and F.-C. Chuang, Anisotropic Rashba splitting in Pt-based Janus monolayers PtXY (X, Y = S, Se, or Te), *Nanoscale Adv.*, **3**, 6608 (2021).
- [12] S.-H. Zhang and B.-G. Liu, Anisotropic Rashba effect and charge and spin currents in monolayer BiTeI by controlling symmetry, *Phys. Rev. B* **100**, 165429 (2019).
- [13] Z. S. Popović, J. M. Kurdestany, and S. Satpathy, Electronic structure and anisotropic Rashba spin-orbit coupling in monolayer black phosphorus, *Phys. Rev. B* **92**, 035135 (2015).

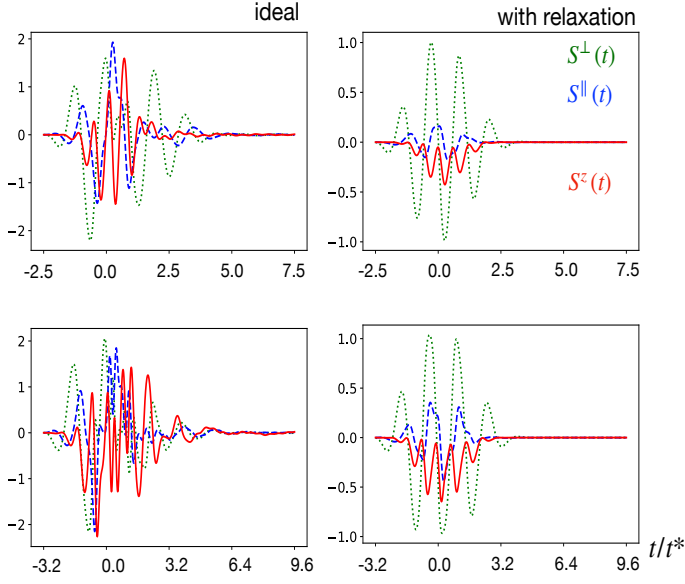


Figure 10: Comparison among different components of the spin polarization, $S^\perp(t)$ (green dotted), $S^\parallel(t)$ (blue dashed) and $S^z(t)$ (red solid) in the ideal situation (left panel) and non-ideal situation (right panel with $\tau = 0.2t^*$). Here we fix the exciting field's polarization to $\varphi_e = 0.25\pi$. The upper panel uses the same set of parameters as those used in Fig. 9. In the lower panel, we have $m_y/m_x = 3.3$, $\varepsilon_F = -0.5\varepsilon_{so}^*$, $E_0 = 1.2E_0^*$, and $\tau_P = 1.6t^*$ with $\omega = (2\pi/t^*)0.625$. Among these, only the out-of-plane component $S^z(t)$ shows constant polarity over time when relaxation effects are accounted (red solid lines in both plots of the right column).